UNIVERSITEIT GENT

FACULTEIT GENEESKUNDE EN GEZONDHEIDSWETENSCHAPPEN

Regulation of the calcium-sensing receptor by amyloid-beta-42: implications for Alzheimer's disease

Jabar Zada Freba

Verhandeling ingediend tot
het verkrijgen van de graad van
Master in de Biomedische Wetenschappen

Promotor: Prof. Dr. *Katharina D'Herde*
Co-promotor: *Dr. Araceli Diez Fraile*
Vakgroep: *Medische Basiswetenschappen*
Dienst Anatomie en Embryologie

Academiejaar 2012-2013

UNIVERSITEIT GENT

FACULTEIT GENEESKUNDE EN GEZONDHEIDSWETENSCHAPPEN

Regulation of the calcium-sensing receptor by amyloid-beta-42: implications for Alzheimer's disease

Jabar Zada Freba

Verhandeling ingediend tot
het verkrijgen van de graad van
Master in de Biomedische Wetenschappen

Promotor: Prof. Dr. *Katharina D'Herde*
Co-promotor: *Dr. Araceli Diez Fraile*
Vakgroep: *Medische Basiswetenschappen*
Dienst Anatomie en Embryologie

Academiejaar 2012-2013

16/05/2013

Jabar Zada Freba *Prof. Katharina D'Herde* *Dr. Araceli Diez Fraile*

Preface

This manuscript has been the effort of a whole team and not one single person. Therefore I would like to take this opportunity to thank all the people who helped me through to accomplish this work.

First of all big thanks to my promotor professor K. D'Herde and my co-promotor Dr. Araceli Diez Fraile (Laboratory of Anatomy and Embryology, UZ Ghent) for their helpful advice and their time spended in critical correction of this thesis. Without them this work would have been impossible.

Further, I would like to thank some other persons from the Laboratory of Anatomy and Embryology who had also their contribution to this work. Very special thanks to Barbara De Bondt and Stefanie Mortier for all their hard work. Above all, thank you for being so supportive and encouraging me in times when I couldn't go further. Thanks to Professor Mark Espeel and Dominique Jacobus for their assistance with the transmission electron microscopy.

Further, I would also like to thank the staff from some other departments who were so kind to help us with their expertise or allowed us to use their equipment.

My special thanks to Tim Lammens and his technicians from the Department of Pediatric Hematology- Oncology and Stamcell Therapy, for their help and guidance with the RT-PCR.

Thanks to Professor Christof Ampe from the Department of Molecular Biology, Institute of Rommelaere, for aiding us with the preparation of oligomeric amyloid-beta peptide.

My gratitude to the staff of Dr. Christopher J. Guérin Laboratory from the Department of Molecular Biomedical Research in VIB (Vlaamse Instituut voor Biotechnologie). They were really helpful while using their confocal microscopy and assisted us a lot to process the images.

I would also like to thank the Department of Histology for allowing us to use their autoclave and liquid nitrogen tube. Furthermore, I would like to thank the Department of physiology for donating us Glial Fibrillary Acidic Protein antibody.

Last but not least, I would like to thank my parents for their unconditional love and support, my brothers and my friends for their encouragement. It was an honor to be a part of such a great project. I hope I have been able to have a small contribution to the research on Alzheimer's disease.

Table of content

State of the art

Alzheimer disease (AD) is the most common irreversible, progressive cause of dementia. It is characterized by a gradual loss of memory and cognitive skills. AD accounts for over 50% of all dementia cases, and today more than 35.6 million people worldwide are affected. Pathological criteria for the diagnosis of AD at autopsy require the demonstration of a sufficient number of neurofibrillary tangles in the neurons and senile plaques in between the neurons on microscopic examination. Senile plaques are mainly composed of aggregates of amyloid-beta (Aβ) peptides.

A vicious cycle may operate to perpetuate activation whereby the Aβ stimulates astrocytes to secrete pro-inflammatory molecules, i.e. interleukin (IL)-1β, tumor necrosis factor (TNF-α) and induced nitric oxide synthase (iNOS) in addition to astrocytic Aβ. Further, several lines of evidence suggest that Aβ may participate in the disruption of cytosolic calcium homeostasis and mechanisms responsible for maintaining intracellular calcium levels, including the calcium-sensing receptor (CaSR), may contribute to AD pathogenesis. Besides, it has been shown that Aβ can activate astrocytes and may act as an agonist of the CaSR. However, little is known about the contribution of CaSR on Aβ-induced astrocyte activation. Thus, the main goal of this work was to evaluate the role of CaSR in astrocyte activation induced by Aβ42 in normal human astrocytes (NHAs).

It has been previously reported that Aβ induces a marked reactive phenotype in astrocytes, changing their flat polygonal shape into stellate, process-bearing morphology and induces cytoskeletal reorganization. First, we evaluated the NHAs for the expression of CaSR. Then the morphological alteration of NHAs upon incubation with Aβ42 or the CaSR agonist NPS-R-568 was evaluated. Lastly, we investigated the secretion of important pro-inflammatory mediators known to be released by astrocytes upon activation with Aβ. Relevant pro-inflammatory mediators released by astrocytes during the late-onset of Alzheimer's disease include IL-1β, TNF-α and iNOS.

In this study we concluded that Aβ42 and NPS-R-568 did neither affect the morphological features nor transcriptional expression of pro-inflammatory mediators of NHA quiescent subcultures. Therefore, although the CaSR is expressed in NHAs, the role of CaSR in astrocyte activation induced by Aβ42 should be further studied.

1. Introduction

1.1. Alzheimer's disease

Originally described by Alois Alzheimer in 1907, Alzheimer's disease (AD) is the most common irreversible, progressive cause of dementia [1,2]. It is characterized by a gradual loss of memory and cognitive skills. AD accounts for over half of all dementia cases, and today more than 35.6 million people worldwide are affected [1,2]. Besides, over five million new cases of AD are reported each year [2]. The prevalence and incidence of AD strongly suggest that age is the most influential known risk factor. Its prevalence increases significantly with age, and its incidence increases to 56.1 per 1000 person years for people above 65 years [2]. Approximately 10 percent of people older than 70 years show memory loss and more than half of these individuals have probably AD. An estimated 45 percent of people older than 85 years have dementia. The duration of disease is typically 8 to 10 years, with a range from 2 to 25 years after diagnosis [2].

1.1.1. Genetics of AD

AD is a complex disorder which involves multiple susceptibility genes and environmental factors. According to age of onset, AD is divided into two subtypes: the early-onset AD (EOAD) and the late-onset AD (LOAD) [1,2]. The EOAD accounts for about 4 percent of all cases and starts from 30 years. However, LOAD, which is the most common form of AD, occurs after the age of 60 years. Both EOAD and LOAD may occur in people with a positive family history for AD [1,2]. About half of EOAD cases is familial and 13 percent of these familial EOAD cases are inherited autosomal dominant with at least 3 generations affected. The EOAD can also occur in families with late-onset disease [2]. Some AD cases in families with autosomal dominant inheritance can be perceived as single-gene disorder. The pattern of transmission is rarely consistent with mendelian inheritance, though the first-degree relatives of patients with LOAD have twice the risk of getting the disease [2].

Overall, more than 90% of patients with AD appear to be sporadic and get the disease in late onset age which is associated with only one gene, the Apolipoprotein E (APOE) gene [1,2]. The early-onset familial forms of AD have an autosomal dominant inheritance linked to 3 genes: amyloid beta precursor protein *(*APP), presinilin-1 (PSEN1*)*, and presinilin-2 (PSEN2), located on chromosomes 21, 14 and 1 respectively [2]. The mechanistic contribution of these genes in AD pathogenesis has been studied extensively, but the specific biology of AD progression remains

unclear [2]. The APOE ε4 is most highly associated with AD for individuals with a family history of dementia. This association is highest for individuals that carry 2 APOE ε4 alleles (ε4/ε4 genotypes). The ε4/ε4 genotype is uncommon. Although the ethnicity of the population may alter the expected prevalence, this genotype occurs in about 1% of normal Caucasian population [1,2].

Both EOAD and LOAD are characterized with a gradual decline of memory. An inability to retain recently acquired information is typically the initial presentation, whereas memory for remote events is relatively spared until later [2]. With disease progression, impairment in other areas of cognition such as language, abstract reasoning, and executive function or decision making occurs to varying degrees. Neurological symptoms that may occur later in the course of illness include seizures, hypertonia, myoclonus, incontinence, and mutism [2].

1.1.2. Structural and functional changes in AD brain

The most important parts of the brain affected by AD are the hippocampus, subiculum and the entorhinal cortex [3]. The brain of a patient with AD often shows marked atrophy, with widened sulci and shrinkage of the gyri. There is often a low brain weight. The loss of weight is more prominent in the cerebrum rather than the brainstem and cerebellum [3]. The brain is affected symmetrically, with the medial temporal lobe worst affected [4]. The lateral ventricles are often enlarged and there is usually a pale locus coeruleus present in the brain. Histopathologically, this disease is characterized by infiltration of inflammatory cells into the central nervous system and neuronal apoptosis [5].

1.1.3. Diagnosis and treatment

Currently, discrimination of AD from other forms of dementia is done through clinical history, neurological examination, and neuropsychological tests [5]. The main condition for diagnosing dementia is the loss of two or more of the following: memory, language, calculation, orientation or judgment [5]. A definitive diagnosis of AD requires a postmortem confirmation, with the presence of two histopathological features: neurofibrillary tangles (NFTs) and amyloid beta (Aβ) plaques [6]. The plaques and tangles are also present in cognitively normal people, but the density of the plaques and the distribution of neurofibrillary tangles are more severe in patients with AD [6]. NFTs are composed of the hyperphosphorylated tau protein [6]. On the other hand, senile plaques are mainly composed of aggregates of Aβ peptides. These Aβ peptides are proteolytic fragments derived from the amyloid precursor protein (APP) which is overexpressed

in AD [7]. Treatment of AD with cholinesterase inhibitors and memantine may result in slowing of cognitive decline in patients with mild-to-moderate dementia, but current treatments do not modify the course of illness [5,6,7].

1.2. Amyloid-beta as cause of AD

In the 1980s, Kang and colleagues purified both plaque and vascular amyloid deposits and isolated 40-residue Aβ peptide, which subsequently led to the cloning of the APP type I integral membrane glycoprotein from which Aβ is proteolytically derived [7]. A new hypothesis the "amyloid hypothesis", was proposed in 1991, which identifies Aβ deposition as the primary cause of AD [7]. This hypothesis suggests that due to overexpression of APP gene, there is an excessive production of Aβ which accumulates around the neurons. The proteolytic processing of the large, transmembrane, amyloid precursor protein (APP) occurs in two distinct amyloidogenic and non-amyloidogenic pathways [8, Fig. 1]. The amyloidogenic pathway involves the sequential cleavage of APP by β-secretase also called beta-site APP cleaving enzyme-1 (BACE-1). This proteinase releases a soluble ectodomain (sAPPβ) and the C-terminal fragment CTF99. A second cleavage by another aspartic proteinase, γ-secretase, generates the transcriptional regulator APP intracellular domain (AICD). Due to its very high ability to aggregation, Aβ forms dimers, trimers, and higher level oligomers which are toxic to cells and cause neuronal death [8]. Formation of amyloid plaques from Aβ aggregates in complex with other proteins is a hallmark of AD. In the non-amyloidogenic pathway APP molecules are cleaved at the α-secretase site within the Aβ-domain releasing a soluble ectodomain sAPPα and the C-terminal fragment CTF83. Proteolytic cleavage of CTF83 by γ-secretase releases AICD and p3 fragment whose functions are still unknown. The AICD fragment, which is produced by APP695 in the amyloidogenic pathway, acts as a transcription factor. AICD from other APP isoforms (APP751 and APP770), produced in the non-amyloidogenic pathway, is most likely to be degraded. Soluble APP ectodomains, sAPPα, and sAPPβ have been shown to have neuroprotective properties [8, Fig.1].

Depending on the point of cleavage by γ-secretase, 2 main forms of Aβ are produced consisting of either 40 or 42 amino acid residues (Aβ40 or Aβ42) [7]. The proportion of Aβ40 to Aβ42 is particularly important in AD because Aβ42 is far more prone to oligomerize and form fibrils than the more abundantly produced Aβ40 peptide. Although it appears that the production of Aβ isoforms is a normal process of unknown function, in a small number of individuals, an increased proportion of Aβ42 is sufficient to cause EOAD [8].

In the past, Aβ has been regarded as acting extracellularly, whereas recent evidence points to toxic effects of Aβ in intracellular compartments [8]. First reports show that Aβ is initially deposited in neurons before occurring in the extracellular space. More recently, it has been shown that neurons in AD-vulnerable regions accumulate Aβ42 and it has been further suggested that this accumulation precedes extracellular Aβ deposition and neurofibrillary tangle formation [9]. Consecutively, a variety of reports has been published demonstrating Aβ in neurons of AD brain. Soluble Aβ oligomers which have been suggested as the most toxic species are formed preferentially intracellular within neuronal processes and synapses rather than extracellularly [9]. In all transgenic mouse models in which marked neuronal loss has been so far reported, this was preceded by considerable amounts of intraneuronal Aβ peptides [9].

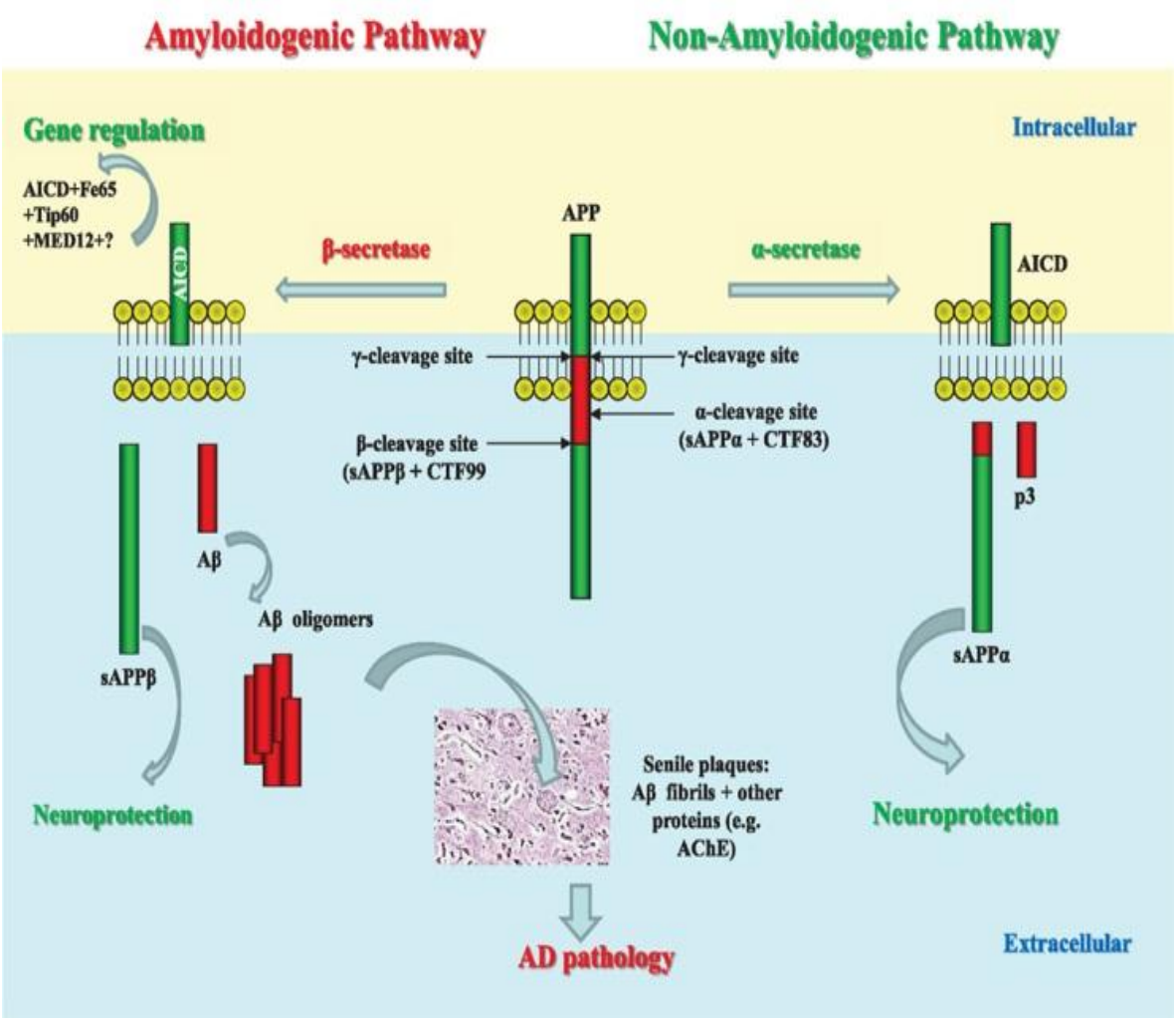

Figure 1. Schematic representation of APP processing and role of its products in AD pathology [8].

1.3. Animal designs for studying AD

Animal models are used to identify disease modifiers, susceptibility genes and to reveal the molecular mechanism of diseases [10]. To better understand the role of Aβ plaques in AD and related disorders, experimental animal models have been developed, which reproduce aspects of the neuropathological characteristics [10]. Their suitability largely depends on the purpose a model has to suit. AD-like neuropathological changes in the brain are commonly the result of aging in long- lived mammals [11]. Extensive Aβ plaques with cognitive impairments were found among domestic dogs, cats and polar bears [11]. However laboratory rats and mice do not show spontaneous aggregations of Aβ deposits with advancing age, but do so when human APP transgenes are overexpressed [11]. This difference is almost certainly due to the fact that the Aβ peptide is well conserved among vertebrates. Further, different species show a different susceptibility to Aβ neurotoxicity. One study has shown that direct injections of Aβ peptides into the brain caused more damage in aged monkeys than in aged rats [11]. The transgenic rats or mice models may offer reproduce more specific aspects of the human disease [10,11]. In addition, transgenic mice present unique and important systems for *in vivo* study of the pathophysiology of a gene of interest [11].

Further, species such as the fruit fly (*Drosophila melanogaster*), the nematode (*Caenorhabditis elegans*), and the sea lamprey (*Petromyzon marinus*) have been employed to provide additional insight into the pathogenesis of AD [9]. Due to their low cost and small size these models are interesting for drug screening and reproducing the cellular biochemistry of neurodegenerative diseases. However, they are less useful to address the behavioral abnormalities of AD. Besides, these lower species have a brain anatomy different from humans, making a direct comparison difficult [9].

Although none of the AD transgenic models fully replicates the human disease, they have suggested new insights into the pathophysiology of Aβ toxicity, particularly with respect to the effects of different Aβ types and the possible pathogenic role of Aβ oligomers [9]. There is now a great interest in understanding the relationship between Aβ and tau pathologies [9]. About 11 APP transgenic mice models have provided strong evidence for the toxicity of soluble Aβ oligomers *in vivo* by showing that many pathological and functional changes in mice occur before the appearance of Aβ plaque pathology [9, table 1].

Table 1. Neuropathological features of the main transgenic mouse models for AD [9].

Mouse model	Gene (mutation)	Intraneuronal Aβ	Parenchymal Aβ plaques	Hyperphos-phorylated Tau	Neurofi-brillary tangles	Neuronal loss	Synaptic loss	CAA	Primary reference
PDAPP	APP (V717F)	-	Yes	Yes	No	No	Yes	-	Games et al. 1995
Tg2576	APP (K670N/M671L)	Yes	Yes	-	-	No	No	-	Hsiao et al. 1996
TgCRND8	APP (K670N/M671L, V717F)	-	Yes	-	No	No	-	-	Chishti et al. 2001
APP/PS1	APP (K670N/M671L), PS1 (M146L)	-	Yes	-	-	-	-	-	Holcomb et al. 1998
APP23	APP (K670N/M671L)	-	Yes	Yes	No	Little	Yes	Yes	Sturchler-Pierrat et al. 1997
Tg-SwDI	APP (E693Q, D694N)	-	Yes	-	-	-	-	Yes	Davis et al. 2004
APPDutch	APP (E693Q)	-	Little	-	-	-	-	Yes	Herzig et al. 2004
APPDutch/PS1	APP (E693Q), PS1 (G384A)	-	Yes	-	-	-	-	Little	Herzig et al. 2004
hAPP-Arc	APP (E693G, K670N/M671L, V717F)	-	Yes	-	-	-	-	Little	Cheng et al. 2004
Tg-ArcSwe	APP (E693G, K670N/M671L)	Yes	Yes	-	-	-	-	Yes	Lord et al. 2006 Knobloch et al. 2007
APPArc	APP (E693G)	-	Yes	-	-	-	-	Yes	Rönnbäck et al. 2011
TAPP	APP (K670N/M671L), Tau (P301L)	-	Yes	-	Yes	-	-	-	Lewis et al. 2001
3xTg-AD	APP (K670N/M671L), Tau (P301L), PS1 (M146V)	Yes	Yes	Yes	Yes	-	No	-	Oddo et al. 2003
APP_{SL}/PS1	APP (K670N/M671L, V717I), PS1 (M146L)	Yes	Yes	-	-	Yes	Yes	-	Wirths et al. 2002
APP/PS1KI	APP (K670N/M671L, V717I), PS1 (M233T/L235P)	Yes	Yes	-	-	Yes	Yes	-	Casas et al. 2004
5xFAD	APP (K670N/M671L, I716V, V717I), PS1 (M146L/L286V)	Yes	Yes	-	-	Yes	Yes	-	Oakley et al. 2006

CAA = cerebral amyloid angiopathy; Dash (-) = not reported.

1.4. Astrocytes

Astrocytes are specialized glial cells that outnumber neurons by over fivefold [12]. They contiguously tile the entire central nervous system (CNS) and exert many essential complex functions in the healthy CNS [12]. Astrocytes are a morphologically heterogeneous population [12,13]. They are divided into two classes termed protoplasmic and fibrous astrocytes [12,13]. Protoplasmic astrocytes are found in gray matter and are characterized by highly complex processes which occupy a large volume [12]. With the light microscope, the fine branches of this process network cannot be resolved. In contrast, fibrous astrocytes, found in white matter, have clearly distinguishable processes with little to moderate branching [12]. Classical and modern neuroanatomical studies also indicate that both astrocyte subtypes make extensive contacts with blood vessels [13]. Electron microscopic analyses have revealed that the processes of protoplasmic astrocytes envelop synapses and that the processes of fibrous astrocytes contact nodes of Ranvier [13]. Both types of astrocytes form gap junctions between distal processes of neighboring astrocytes [12,13].

1.4.1. The role of astrocytes

Astrocytes have traditionally been thought to serve others in the nervous system and to regulate and optimize the environment within which neurons function [13]. They maintain tight control on local ion and pH homeostasis, deliver glucose and provide metabolic substrates to neurons. They also clean up neuronal wastes, such as metabolic byproducts and neurotransmitters released during synaptic transmission. In other words, they are multifunctional housekeeping cells [13].

Another important characteristic of astrocytes is their capability to repair and form wound after traumatic or inflammatory injuries [13]. Astrocytes are activated to display "reactive astrogliosis" around site of injury, a process that leads to excessive wound formation and interferes with the neuronal recovery process. The sensitive reactivation process and the inducible overproduction of pro-inflammatory mediators make astrocyte a very important contributor to the neuro-inflammation in the early stage of AD pathogenesis [13].

In addition, under stress and injury, astrocytes become astrogliotic leading to an upregulation of the expression of pro-inflammatory cytokines and chemokines, which are associated with the pathogenesis of AD [13]. Reactive astrocytes or astrogliosis is a reliable and sensitive marker of diseased tissue. Although reactive astrogliosis is used widely as a pathological hallmark of diseased CNS tissue, definitions of reactive astrogliosis can vary considerably among authors and there are no widely accepted categories of intensity or severity. Based on a large body of observations in experimental animals, a definition of reactive astrogliosis has recently been proposed that encompasses four key features [13]. Reactive astrogliosis is a spectrum of *potential, molecular, cellular* and *functional* changes in astrocytes that occur in response to all forms and severities of CNS injury and disease [13].

1.4.2. Astrocytes and Aβ in AD

Amyloid-beta can be generated from both astrocytes and neurons through the stimulation with various cytokines [14]. This means that astrocytes can be induced by pro-inflammatory stimuli to produce Aβ. It has been demonstrated that interferon-gamma (IFN-γ) in combination with tumor necrosis factor-alfa (TNF-α) or interleukin-1β (IL-1β) can induce primary human astrocytes or astrocytoma cells to produce Aβ [14].

On the other hand, several lines of evidence suggest that Aβ can activate astrocytes and that the inflammatory response induced upon astrocyte activation is a critical component in AD [15]. As astrocytosis is one of the characteristic features in the AD brain, Aβ production by astrocytes may substantially contribute to the Aβ load. Activated astrocytes can produce IL-1β, TNF-α and induced nitric oxid synthase (iNOS) [15].

This whole process works in a vicious cycle where Aβ can as well stimulate astrocytes as being produced by astrocytes [figure 2]

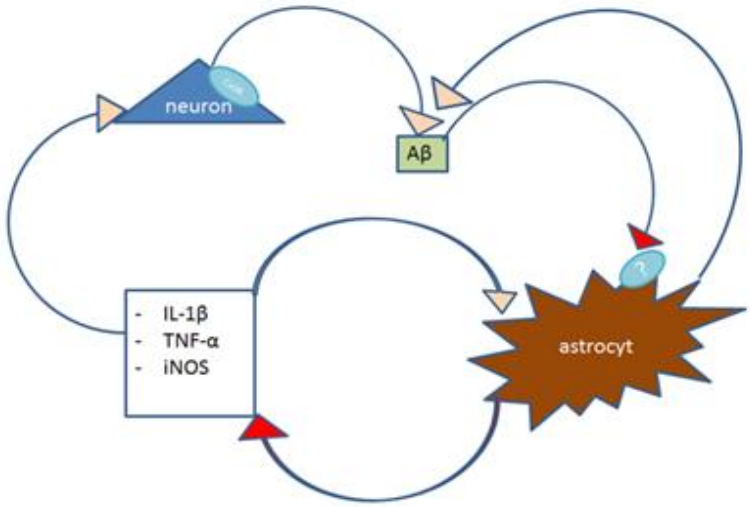

Figure 2. Schematic representation of vicious cycle between Aβ, astrocyte, neuron and pro-inflammatory mediators; IL-1β, TNF-α and iNOS.

1.4.3. Pro-inflammatory mediators induced by astrocytes

IL-1β has been documented to play a role in neuronal degeneration. In astrocytes, IL-1β induces IL-6 production, stimulates iNOS activity. In addition, IL-1β enhances microglial and astrocyte activation and additional IL-1β production [15].

TNF-*α* plays a central role in initiating and regulating the cytokine cascade during an inflammatory response [16]. It is produced as a membrane-bound precursor molecule of 26 kDa that is cleaved by the TNF-*α* converting enzyme to produce a 17 kDa active cytokine [16]. The levels of TNF-*α* expression in the healthy brain are low, making it difficult to determine its precise role under physiological conditions. In inflammatory or disease states, TNF-*α* along with several other pro-inflammatory mediators are predominantly produced by activated astrocytes

[16].

1.5. Calcium homeostasis and AD

Calcium acts as an extra- and intracellular messenger molecule mediating adaptive changes in neuroarchitecture in response to signals such as neurotransmitters and neurotrophic factors [17]. In the brain, calcium is also involved in long-term adaptive processes, such as memory [17]. Such adaptive changes require an optimal range of intracellular Ca^{2+} (Ca_i^{2+}) and play major roles during development and in the plasticity of the adult nervous system. Calcium homeostasis in the CNS is maintained by Ca^{2+} entry into neural cells, Ca^{2+} release from the endoplasmatic reticulum (ER) and mitochondria [17].

The disruption of calcium homeostasis is an alternative hypothesis of AD etiology or a significant mechanism in the pathological cascade of the disease [18]. There are many scientific studies pointing to calcium as a main player in neurodegenerative diseases such as AD. Support for this hypothesis includes the observation that calcium ion (Ca^{2+}) levels, outside of the normal physiologic range, result in neuronal cell death [18]. Additional support for calcium involvement in AD pathogenesis comes from the fact that calcium ions play a key role in normal neuronal function. For instance, Ca^{2+} regulates synaptic plasticity. Besides, increases in intracellular Ca^{2+} result in prevention of microtubule and microfilament assembly in neurons, and the presence of elevated extracellular Ca^{2+} facilitates more rapid expression of neuronal injury than when extracellular Ca^{2+} levels are normal [18]. Ca^{2+} levels are known to modulate neurotransmitter release, neuronal membrane excitability and it participates in neuronal gene regulation. Calcium dysregulation is further implicated in AD since each of the genes currently known to influence AD susceptibility so far (APP, PSEN1, PSEN2, and APOE) affects intracellular Ca^{2+} levels and/or calcium signaling [18]. Since Ca^{2+} concentration plays such an important role in normal neuronal function, abnormal Ca^{2+} levels and calcium signaling produce symptoms of brain aging, neuronal degeneration and death. Then mechanisms responsible for maintaining Ca^{2+} levels may contribute to AD susceptibility, including the calcium sensing receptor (CaSR) [18].

1.5.1. The calcium-sensing receptor (CaSR)

CaSR is a G-protein coupled (GPCR), transmembrane receptor [17-18]. It is expressed in tissues involved in calcium homeostasis such as the parathyroid and kidney. In addition, it is also expressed in quail granulosa explants [19] and in tissues where its function is less readily

apparent, such as the brain [17-18].

The human CaSR has three structural domains: N-terminal extracellular domain (ECD), the transmembrane domain (TMD) with 7 helices (7 TM), and a hydrophilic intracellular C-terminal domain [20].

Several splice variants of the CaSR gene have been described in the literature. A cDNA clone of the human parathyroid CaSR has been found which contains a 30-nucleotide insertion within the region of the gene encoding the receptor's ECD [20]. This 10-amino acid insertion had no apparent effect on the function of the CaSR as assessed by expression in *Xenopus laevis* oocytes [20]. The same splice variant has also been identified in human breast cancer tissue [20]. Its functional significance requires further investigation. Another alternatively spliced CaSR transcript which is expressed in human cytotrophoblasts and parathyroid lacks exon 3 and encodes for an inactive receptor [20]. Whether this receptor can interfere with the normal CaSR function is to be determined. Another alternatively spliced form of the CaSR in keratinocytes has also been described. This spliced variant lacks exon 5, producing an in-frame deletion of 77 amino acids and resulting in an expressed protein which is smaller and exhibits an altered glycosylation pattern compared to the full-length CaSR [20]. The truncated CaSR was inactive when it was transfected into Human embryonic kidney (HEK293) cells or keratinocytes. In addition, it interfered with the function of the co-expressed full-length CaSR [20]. This latter observation may explain the reduced responsiveness of differentiated keratinocytes to extracellular Ca^{2+}-induced elevations of intracellular Ca^{2+}. The alternatively spliced form of CaSR is expressed at higher levels in the differentiated cells and could exert a dominant negative action on the full-length CaSR expressed within the same cells [20]. Finally, there can be alternative splicing within the 59-untranslated region (UTR) of the CaSR gene. For instance, transcripts in human parathyroid vary within their 59-UTRs, consistent with alternative splicing of noncoding exons within the 59-upstream region of the gene, without, however, altering the coding region [20]. Such alternative splicing within the gene's putative upstream regulatory regions could clearly participate in tissue-specific expression and/or regulation of the CaSR gene, however, further studies are needed to define its importance in this regard [20].

1.5.2. CaSR in the brain

CaSR has been localized to almost all areas of brain, with varying degrees of abundance. It is widely expressed in central nervous system, mostly scattered in cerebellum, brainstem, corpus callosum, hippocampus and lateral orbital cortex [20]. It is highly present in subfornical organ and olfactory bulbs. Further, it is also expressed in oligodendrocytes, neurons, microglia and astrocytes of different species [20]. CaSR is regulating various aspects of cellular function within the CNS. In neurons, the CaSR could be involved in the maintenance of membrane potential , regulation of ion channels and long term potentiation. It was recently shown that the CaSR is expressed in the astrocytoma cell line U87 [20]. Although an earlier study failed to detect expression of the CaSR in primary astrocytes isolated from rat brain, Brown et al. were able to demonstrate the presence of CaSR mRNA and protein in primary human astrocytes [21].

1.5.3. The role of CaSR in AD

It has been reported that AD patients demonstrate altered systemic calcium homeostasis in relation to normal age-matched controls, including a decrease in serum calcium level, increase in urinary calcium excretion, and a decrease in serum 1,25-dihydroxy-vitamin D concentration [18]. Additionally, the signal transduction cascade, initiated by CaSR activation, involves inositol triphosphate (IP3), phospholipase C (PLC) production and protein kinase C (PKC). The levels of these three molecules are altered in the Alzheimer brain [18]. This means that, the level of CaSR activation may directly affect signal transduction, mobilization of intracellular Ca^{2+} stores, and subsequent calcium channel activation in brain tissue, disrupting local Ca^{2+} homeostasis [18].

The large extracellular N-terminal of CaSR contains a bilobed venus flytrap (VFT) domain and a cysteine-rich domain [22]. The VFT domain is homologous to bacterial periplasmic binding proteins and it is involved in agonist binding. The VFT undergoes structural changes when an agonist binds to the cleft of its lobes [22].

The CaSR can be activated by amino acids, extracellular Ca^{2+}, Mg^{2+} and antibiotics [23, figure 3]. Further, it responds to various endogenous agonists present in the brain, such as polycationic agonists or organic polyamines, including spermine and spermidine [23]. In addition NPS R-568 (*N*-(3-[2-chlorophenyl]propyl)-(*R*)-a-methyl-3-methoxybenzylamine), a synthetic allosteric modulator of CaSR, has been shown to decrease plasma levels of parathyroid hormone (PTH) in rats. In addition it was also shown that NPS-R-568 increases calcitonin secretion through its activity at 7 TM of CaSR on parathyroid cells [23].

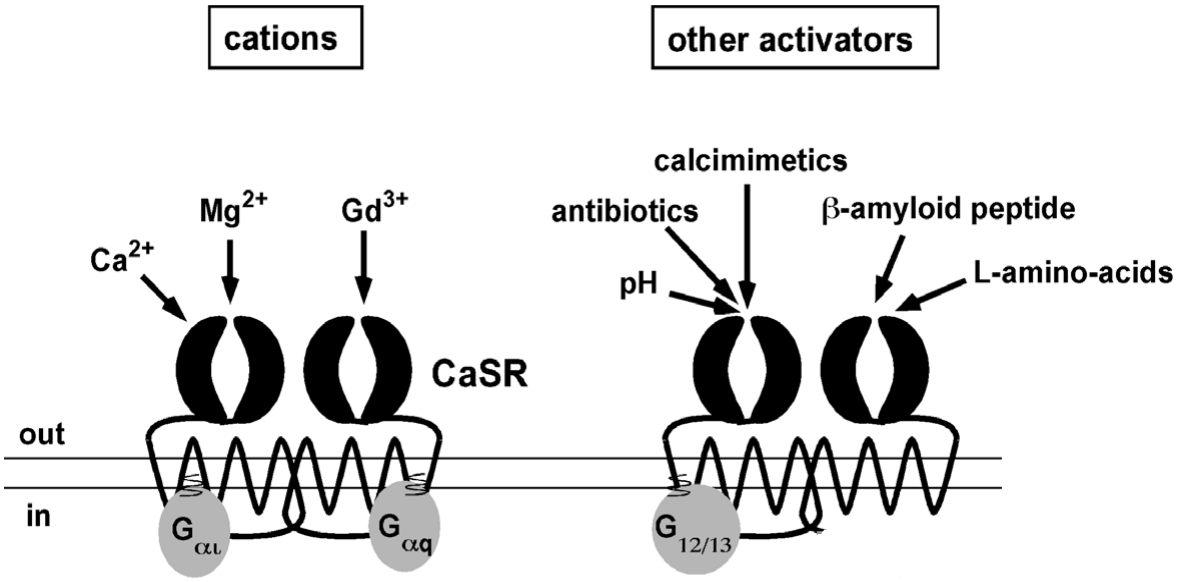

Figure 3. (poly)cations: Calcium (Ca^{2+}), Magnesium (Mg^{2+}), Gadolinium (Gd^{3+}), calcimimetics, amino-acids, antibiotics, pH and Aβ-peptide stimulate CaSR activity leading to the recruitment of multiple intracellular pathways [24]. Out = extracellular space, in = intracellular space

Recently, Aβ has also been identified as a CaSR agonist [25]. The interaction has been proposed to occur at the orthosteric site of the CaSR by means of the Aβ-positively charged side chains [22-25]. The major physiological function of CaSR is systemic calcium homeostasis, however, little is known about CaSR function in the brain [25].

Recent lines of evidence indicate that CaSR is a potential target for Aβ-mediated disturbances in the events resulting in altered levels of calcium in neurons and participating in the activation of induced nitric oxide synthase (iNOS) in activated astrocytes by cytokines, leading to the slow development of late-onset Alzheimer's disease [26]. Remarkably, incubation in the presence of CaSR-agonists is able to mediate the release of pro-inflammatory mediators such as TNF-α and NO in kidney cells and Leydig cancer cells, respectively [27].

Although it has been shown that Aβ can activate astrocytes and may act as an agonist of the CaSR, little is known about the contribution of CaSR on Aβ-induced astrocyte activation. Thus, the main goal of this work is to evaluate the role of CaSR in astrocyte activation induced by Aβ42 in normal human astrocytes (NHAs).

1.6. Hypothesis

It is believed that abnormal processing of the APP results in different Aβ fragments, the most toxic of which is the Aβ42 peptide. A vicious cycle may operate to perpetuate activation whereby the Aβ stimulates astrocytes to secrete pro-inflammatory molecules, i.e. interleukin-1β (IL-β), tumor necrosis factor-alfa (TNF-α) and induced nitric oxide synthase (iNOS) in addition to astrocytic Aβ [28]. Although deposition of Aβ42 peptide clumps in the brain is one of the primary causes of neuronal loss in AD, mechanisms by which Aβ causes neurodegeneration are not well understood. Several lines of evidence suggest that Aβ may participate in the disruption of cytosolic calcium homeostasis in AD. The intracellular calcium regulates synaptic plasticity, modulates neurotransmitter release and neuronal membrane excitability [18]. Since intracellular calcium concentration plays such an important role in normal neuronal function, then abnormal calcium levels and calcium signaling lead to symptoms of brain aging, neuronal degeneration and neuronal death [18]. Thus, mechanisms responsible for maintaining intracellular calcium levels, including the calcium-sensing receptor (CaSR), may contribute to AD pathogenesis [18].

Within this research project we sought to improve our understanding of the involvement of CaSR on Aβ-induced activation in normal human astrocytes. We hypothesized that CaSR is implicated in Aβ42-mediated activation of human astrocytes.

First, we evaluated the involvement of the CaSR in Aβ-mediated morphological activation of human astrocytes. To determine the involvement of the CaSR in Aβ-mediated morphological activation, NHAs were cultured in the presence of Aβ or the CaSR agonist NPS-R-568. It has been previously reported that Aβ induces a marked reactive phenotype in astrocytes, changing their flat polygonal shape into stellate, process-bearing morphology and induces cytoskeletal reorganization [29,30].

Secondly, we investigated the secretion of important pro-inflammatory mediators known to be released by astrocytes upon activation with Aβ. Relevant pro-inflammatory mediators released by astrocytes during the late-onset of Alzheimer's disease include IL-1β, TNF-α and iNOS [30].

2. Materials and methods

2.1. Reagents

Commercially available human amyloid beta 1-42 (Aβ42, Advanced Chemtech, Louisville, Kentucky, USA) was initially dissolved at a concentration of 1 mg/ml in 100% 1,1,1,3,3,3-hexafluoro-2-propanol (HFIP, Carl Roth, Karlsruhe, Germany). This solution was incubated at room temperature for one hour, with occasional vortexing at moderate speed (Figure 4). Next, the solution was sonicated for 10 minutes in a water bath sonicator. The HFIP/peptide solution was then dried under a gentle stream of nitrogen gas and subsequently resuspended in dimethyl sulfoxide (DMSO, Sigma, Steinheim, Germany) to a concentration of 5 mM. This solution was incubated at room temperature for 12 minutes with occasional vortexing. The final solution was then aliquoted in 35 µl DMSO and stored at -80°C. For a working solution each aliquot was diluted in 1715 µl D-PBS (Dulbecco's Phosphate-Buffered Saline, Life technologies, Belgium) to obtain a 100 µM stock. This solution was incubated at 4°C overnight to allow for peptide aggregation. The employed reagent handling has been previously described to give raise to the oligomeric state of amyloid beta according to Abcam's instructions.

The CaSR positive allosteric modulator, NPS-R-568 (Tocris, Bioscience, Bristol, UK) was dissolved in DMSO at 20 mM and then stored in aliquots at -80°C.

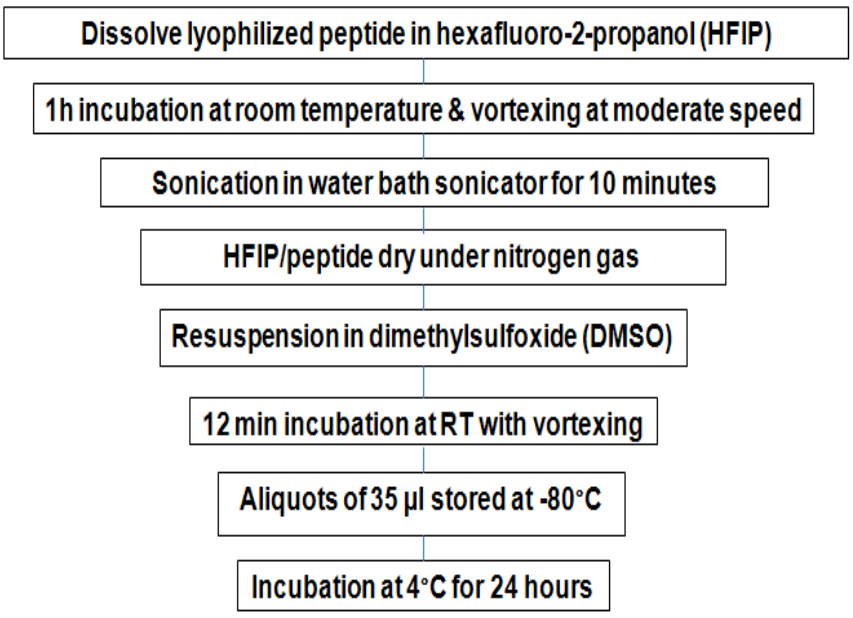

Figure 4. Schematic diagram summarizing the handling for preparing oligomeric Aβ42.

2.2. Astrocyte culture and experimental protocol

A T25 culture flask of proliferating CC-2665 Normal Human Astrocytes (NHA) was purchased from Lonza (Basel, Zwitserland). Cells were cultured in astrocyte growth medium AGM™ BulletKit™ (Lonza, Basel, Zwitserland) according to manufacturer's instructions under standard culture conditions at 37°C in 5% CO_2-enriched atmosphere. Clonetics™ AGM™ BulletKit™ consists of a 500 ml bottle of Astrocyte Basal Medium (ABM™) and the following supplements: 0.5 ml of recombinant human epidermal growth factor (rhEGF), 1.25 ml of insulin, 0.5 ml of ascorbic acid, 0.5 ml of gentamicin (GA-1000), 5 ml of L-Glutamine and 15 ml of FBS. CaSR is functionally insensitive when extracellular Ca^{2+} concentration is lower than 1mM [19]. The final Ca^{2+} concentration in AGM was 240 mg/l (1.63 mM). Thus, theoretically, a sufficient concentration of Ca^{2+} was added to the medium used during quiescence, even when the quiescence medium was diluted in D-PBS, reaching a Ca^{2+}-concentration of 1.3 mM.

When cultures reached a confluency of circa 80% the cells were trypsinized and their viability was evaluated using the trypan blue dye exclusion staining. Astrocytes were subsequently subcultured with a seeding density of 5,000 living cells/cm² in T25 or T75 culture flasks. Astrocytes from the fifth subculture were cryopreserved in 2 ml vials using 10% DMSO, 10% FBS and 80% AGM with at least one million living cells in a total volume of 1 ml. The cryovial was first incubated overnight in isopropanol and then kept in liquid nitrogen (Air liquid Belux, Luik, Belgium). Cells were thawed and used consistently at their seventh subculture for the experiments.

NHA subconfluent cultures from the sixth subculture were trypsinized and plated on 24 well plates on glass coverslips for RNA analysis and immunocytochemistry experiments, or into four well Nunc dishes (1.9 cm²/well, Nunc, Roskilde, Denmark) for transmission electron microscopy (TEM) at a density of 10,000 living cells/cm². Once the cultures reached a confluency of circa 90% astrocytes were incubated for 24 hours in quiescence medium, consisting of 0.5% FCS, 1.4% supplements and 98.1% ABM. Astrocytes were then incubated either with oligomeric Aβ42 (at 1, 10, 20 µM) or R-568 (at 0.1, 1, 10 µM). Vehicle was 0.4% and 0.01% DMSO for Aβ42 and R-568, respectively. Cultures were sampled at 6 and 12 hours after the onset of amyloid beta or R-568 agonist exposure. Initially, the cultures were rinsed twice in PBS at 37°C. Then some cultures were fixed in 4% paraformaldehyde (Merck, Darmstadt, Germany) in PBS (pH 7.4) rinsed in PBS and stored at 4°C for immunocytochemical and actin staining. Other samples were collected in Qiazol® Lysis Reagent (Qiagen, Hilden, Germany) and immediately stored at -80°C for mRNA

evaluation. Some cultures were fixed in 4% formol (Sigma, St-Louis, USA) in cacodylate (pH 7.4) for transmission electron microscopy. This experimental setup was repeated four times.

2.3. Immunocytochemical staining

Calcium-sensing receptor

Since this NHA cell line has not been completely characterized, we determined the level of expression of CaSR on these cells. The CaSR protein was identified by immunofluorescence with the mouse anti-CaSR monoclonal antibody (mAb) ADD against amino acids 214–235 of the extracellular domain of the human parathyroid CaSR (Abcam, Cambridge, UK). Mat Tech's® glass bottom culture dishes (MatTek Corporation, Ashland, USA) were used to carry out this experiment because they allow to produce high-resolution microscopic images of cultured cells. Subconfluent NHA cultures were rinsed twice with PBS at 37°C, fixed in 4% paraformaldehyde for 15 minutes at room temperature. The intracellular CaSR was detected upon permeabilization of the NHA subcultures with 0.5 % Triton X-100 (Merck, Darmstadt, Germany) while non-permeabilized cells were used to evaluate the presence of extracellular CaSR. Each slide was blocked with 3% BSA (Roche, Manheim, Germany) and 1% glycine (Merck, Darmstadt, Germany) during 20 minutes at room temperature and then washed 3 times with 1% BSA. Afterwards, the cells were incubated in 10% rabbit-serum (Sigma-Aldrich, Steinheim, Germany) during 30 minutes at room temperature. The primary antibody was added for one hour at room temperature at a concentration of 3.5 µg/ml immediately after blocking without washing the cells. Mouse IgG2a (DAKO, Glostrup, Denmark) was used as a nonbinding isotype negative control at the same concentration as the CaSR antibody. The cells were then washed three times during five minutes with 1% BSA in PBS and incubated with Alexa-fluor-488 rabbit-anti-mouse IgG secondary antibody (10 µg/ml, Molecular probes, Oregon, USA) in 1% BSA for 45 minutes at room temperature. Then, the cells were rinsed three times during five minutes with PBS. Staining of cellular nuclei was carried out using 4',6-diamidino-2-phenylindole (DAPI, Sigma Aldrich, Steinheim, Germany) at a final concentration of 1 mg/ml for 3 minutes at room temperature. Samples were covered with Mowiol® 4-88 (Calbiochem, San Diego USA) supplemented with 25 mg/ml 1,4-diaza-bicyclo(2.2.2)octane (DABCO; Sigma). Freshly isolated human granulosa cells (Ethical approval N°B67020109143) were used as positive control since they have been described to stain positive for the CaSR [31]. Dishes were kept in the dark at 4°C until examined. Cellular

presence of CaSR protein in combination with DAPI staining was examined by confocal microscopy (Leica Microsystems, Groot-Bijgaarden, Belgium).

The intracellular and extracellular disribution of CaSR is studied by means of a Leica TCS SP5 confocal laser scanning microscope (CLSM). There was one magnification used, namely, 40x, HC PL Apo 0.7 IMM. Ultraviolet diode, with a wave length of 405 nm, was used as a laser for the excitation of DAPI staining. DAPI has a light absorbing capacity around 358 nm and causes emission of blue light around 500 nm. AF488 absorbs light around a wavelength of 495 nm and causes emission of green light by 519 nm. The images were combined and processed with Volocity (PerkinElmer, Zaventem, Belgium).

Glial Fibrillary Acidic Protein

Cultured NHA were fixed with 4% paraformaldeyde (PFA, Merck, Darmstadt, Germany) and permeabilized with 0.1% Triton X-100 in PBS (pH 7.4). Fluorescent immunocytochemistry staining was performed on cells blocked with 10% sheep serum (S3772, Sigma-Aldrich, Steinham, Germany) over 1 hour at room temperature using anti-GFAP primary antibody (Abcam 7260, Cambridge, UK) at 1/500. Subsequently incubation with sheep anti-rabbit Dylight-488 (STAR36D488, Abd Serotec, Kidlington, UK) secondary antibody at 1/1000 was performed. As described above nuclei were stained with DAPI. Staining was examined by fluorescence microscopy and images were obtained with a digital camera (Nikon Digital Sight DS-5M, Tokyo, Japan). The images were combined and processed with Paint.Net (version 3.5.6).

2.4. Actin Staining

The cells were fixed with 4% PFA and rinsed in PBS (pH 7.4) further treated with 0.5 % Triton X-100 for 10 minutes at room temperature and washed three times with PBS. The F-actin of the cultured cells was stained with Rhodamine-phalloidin conjugated to tetramethylrhodamine (TRITC, Sigma-Aldrich, Steinheim, Germany) during 5 minutes at room temperature in dark and three times washed with PBS. Staining of nuclei was carried out using DAPI and samples were processed as described in the previous paragraph. The images were taken at random starting from the upperside of the slide and going down and this counter-clockwise.

2.5. Transmission Electron Microscopy

Cultures in nunc dishes were fixed in a solution of 1% aqueous osmiumtetroxide in 0.1 M natrium-cacodylate buffer (pH 7.4) overnight at 4°C. Osmicated cultures were dehydrated through a graded series of ethanol, and embedded in LX-112 (Ladd Research Industries, Williston, USA). The polymerization of LX-112 was performed in an oven at 60°C during 48 hours. Subsequently a semithin orientation section of 2 µm was cut and brought into a drop of milli-Q water on a slide. This slide was placed on a warm plate so that the drop was evaporated and the section attached on the bottom. A non-specific toluidine blue staining was performed to increase the contrast. Afterwards the slide was observed under the microscope and the specific region for further processing was selected. From this block, ultrathin sections of 80 nm were cut with a diamond blade put on the microtome (Ultracut E, Reichert-Jung). These sections were mounted on copper grids (2 mm x 1 mm slot, Agar Scientific, Essex, England) carrying a homemade Formvar film and stained with uranyl acetate and lead citrate. Imaging was performed at an acceleration voltage of 80kV using a JEOL EXII transmission electron microscope (JEOL Ltd, Zaventem, Belgium). Negatives were scanned and further processed with Adobe Photoshop version 8.0.

To distinguish the fibrillar-amyloid-beta from the oligomeric form, the following method was used. Aliquots of sample (5 µl) were pipetted on to the surface of carbon-coated electron microscope grids and adsorbed for 2 minutes at room temperature. After rinsing with 20 µl of sterile deionized water, 5 µl of 1% (w/v) uranyl acetate was added for 15-20 seconds as a negative staining. Grids were then blotted dry and examined under transmission electron microscope.

2.6. RNA extraction, reverse transcription quantitative RT-PCR (qRT-PCR)

The CaSR mRNA levels from the third to the seventh subculture were evaluated by RT-qPCR. In addition mRNA levels of three pro-inflammatory mediators i.e. interleukin-1β (IL-1β), induced nitric oxid synthase (iNOS) and tumor necrosis factor-α (TNF-α) were also evaluated by RT-qPCR.

Total RNA was isolated using the miRNeasy mini kit (Qiagen, Valencia, CA, USA) according to the manufacturer's instructions. For each sample, RNA concentration was measured using the NanoDrop ND-1000 (NanoDrop Technologies, Wilmington, DE, USA). The cDNA was generated using the Superscript III First Strand synthesis systems for RT-qPCR (Invitrogen) according to the instructions of the manufacturer. Reactions were performed using 200 ng RNA. After cDNA preparation, the samples were diluted 2-fold and stored at -20°C. qRT-PCR reactions

were performed in a total volume of 5 µl. The reaction mix contained 1 µl of diluted cDNA, 2.5 µl of TaqMan Universal Master Mix (2x), 1 µl TaqMan primer-probe mix and 0.5 µl water. Reactions were carried out on a ViiA7 qRT-PCR machine (Applied Biosystems). Reactions were performed in triplicate. Expression of GAPDH and HPRT-1 was used for normalization and relative expression values were calculated using the ΔCt-method. The following primer-probe mixes were used: GAPDH (Hs02758991_g1), HPRT-1 (Hs02800695_m1), IL-1β (Hs01555410_m1), TNF-α (Hs01113624_g1), iNOS (NOS-2α, Hs01075529_m1) and CaSR (Hs01047793_m1) from Applied Biosystems.

3. Results

3.1. Morphology and CaSR expression in resting subconfluent NHA cultures

NHA cells were brought into resting conditions by incubating subconfluent cells for 24 hours in quiescent medium. NHA cultures under the defined conditions are characterized by a morphological heterogenity as evidenced by fluorescence microscopy upon actin filament staining (Fig. 5). A large proportion of cells look flat, polygonal and show long, thin processes. While some other cells which also appear abundantly, look rounded and carry no processes. A characteristic stellate (star shaped) feature is not visible in these cells, though most cell nuclei are typically rounded. Some nuclei are located on the processes of the cells instead of in the cell body. The actin filaments, within each cell, are mostly parallel and oriented to one direction.

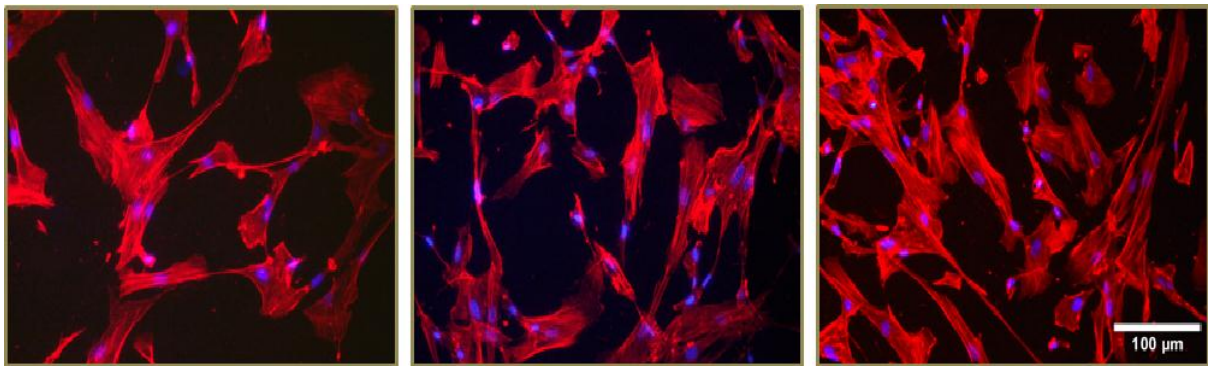

Figure 5. Three representative images, out of five different biological replicates, from resting NHA subconfluent cultures, after 24 hours incubation in quiescent medium. TRITC-phalloidin (red) staining is used to visualize the redistribution of F-actin cytoskeleton and DAPI (blue) staining is used to visualize the cellular nuclei. The pictures are taken with 20x objective.

Ultra-structural observation of resting NHA subcultures revealed cells with ovoid or irregular nucleus with the nuclear envelope thrown into deep folds (Fig. 6a, c). Occasionally, a nucleolus is present. In the cytoplasm, we could identify zones with closely packed fibrils with a diameter of circa 8 to 9 nm, appearing hollow in transverse sections and some microtubule with a diameter of circa 25 nm were observed (Fig. 6b, d).

Under the current culture conditions, glycogen storage, a typical aspect for astrocytes *in vivo* was limited to the presence of accumulations of monoparticulate β glycogen particles (Fig. 6d). In the cytoplasm elongated mitochondria, rough endoplasmatic reticulum, free ribosomes and lipid droplets could be seen (Fig. 6b, c, d). At the plasma membrane invaginations with the typical

morphology of coated vesicles are present. Occasionally, areas with a high number of regularly placed microvesicles with a diameter between 50 and 60 nm are seen, suggestive for plasmalemmal vesicles or caveolae (Fig. 6b). Cytoplasmic flat extensions in the form of sheets containing fibrils and no other organelles were sometimes observed (Fig. 6e). More frequently, cytoplasmic extensions appear elongated, with rounded to oval profiles on transverse section (Fig. 6c). At some places very close contact between opposing cytoplasmic extensions were seen and gap junctions could be photographed (Fig. 6f). The described ultra-structural features are in accordance with the morphological characteristics of fibrous astrocytes as described *in vivo*, although the cytoplasmic flat extensions are more characteristic for protoplasmic astrocytes.

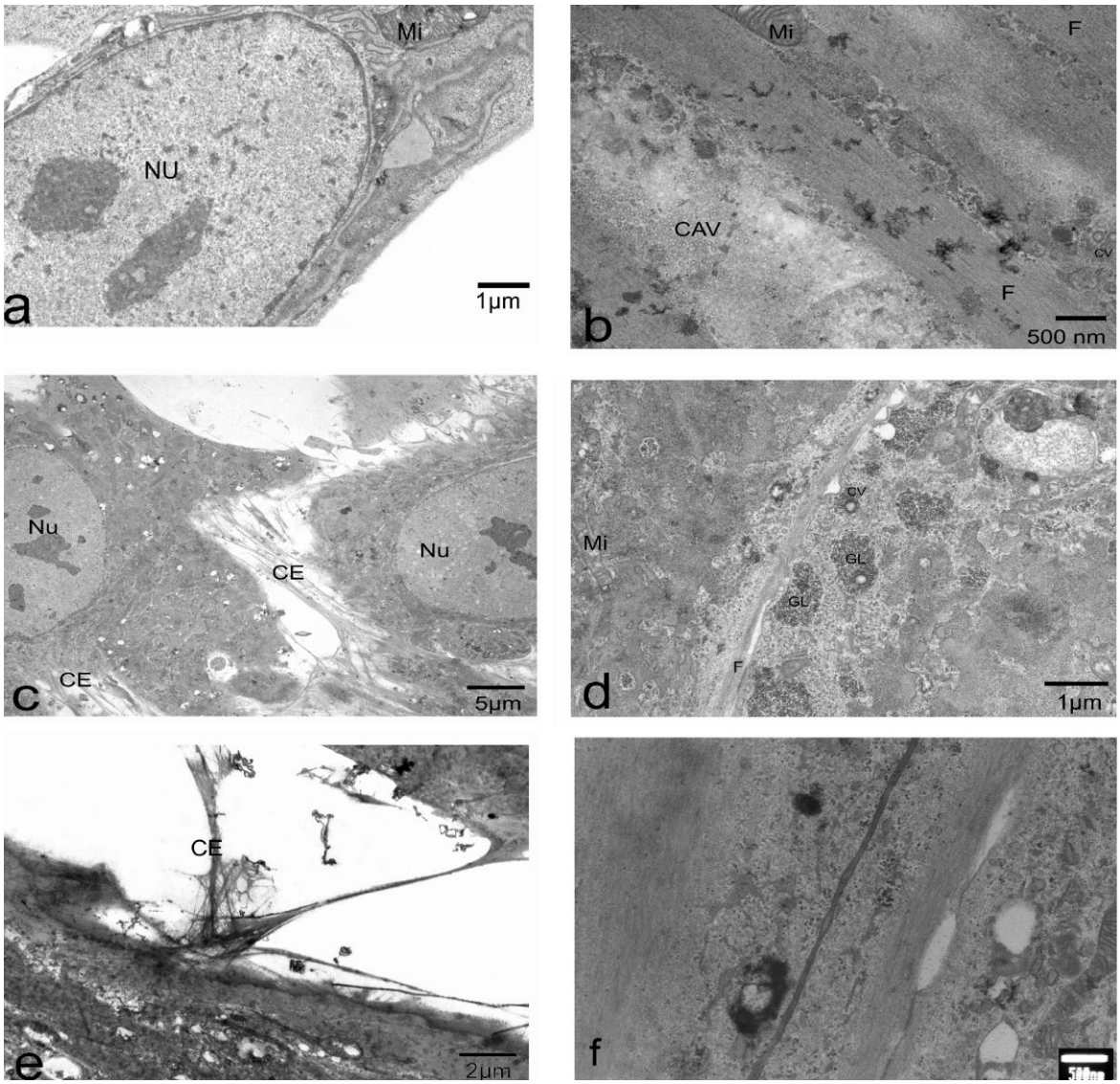

Figure 6. Ultra-structure of NHA subconfluent cultures in resting conditions visualized by transmission electron microscopy. Nucleus (Nu), Mitochondrion (Mi), Caveolae (CAV), fibril (F), cytoplasmic extension (CE), coated vesicle (CV), β glycogen particle (GL).

CaSR protein expression in resting NHA subconfluent cultures (Fig. 7) was evaluated by confocal microscopy. Negative controls did not show any expression of CaSR protein (Fig. 7A, B). While non-permeabilized NHA subcultures (Fig. 7C) showed a low expression of CaSR, a higher expression was detected in permeabilized subcultures (Fig. 7D). This observation indicates that an important proportion of NHA cultures expresses the CaSR at the cellular membrane and possesses a relevant intracellular pool of this protein. However, we were not able to detect any expression of CaSR mRNA by qRT-PCR (data not shown).

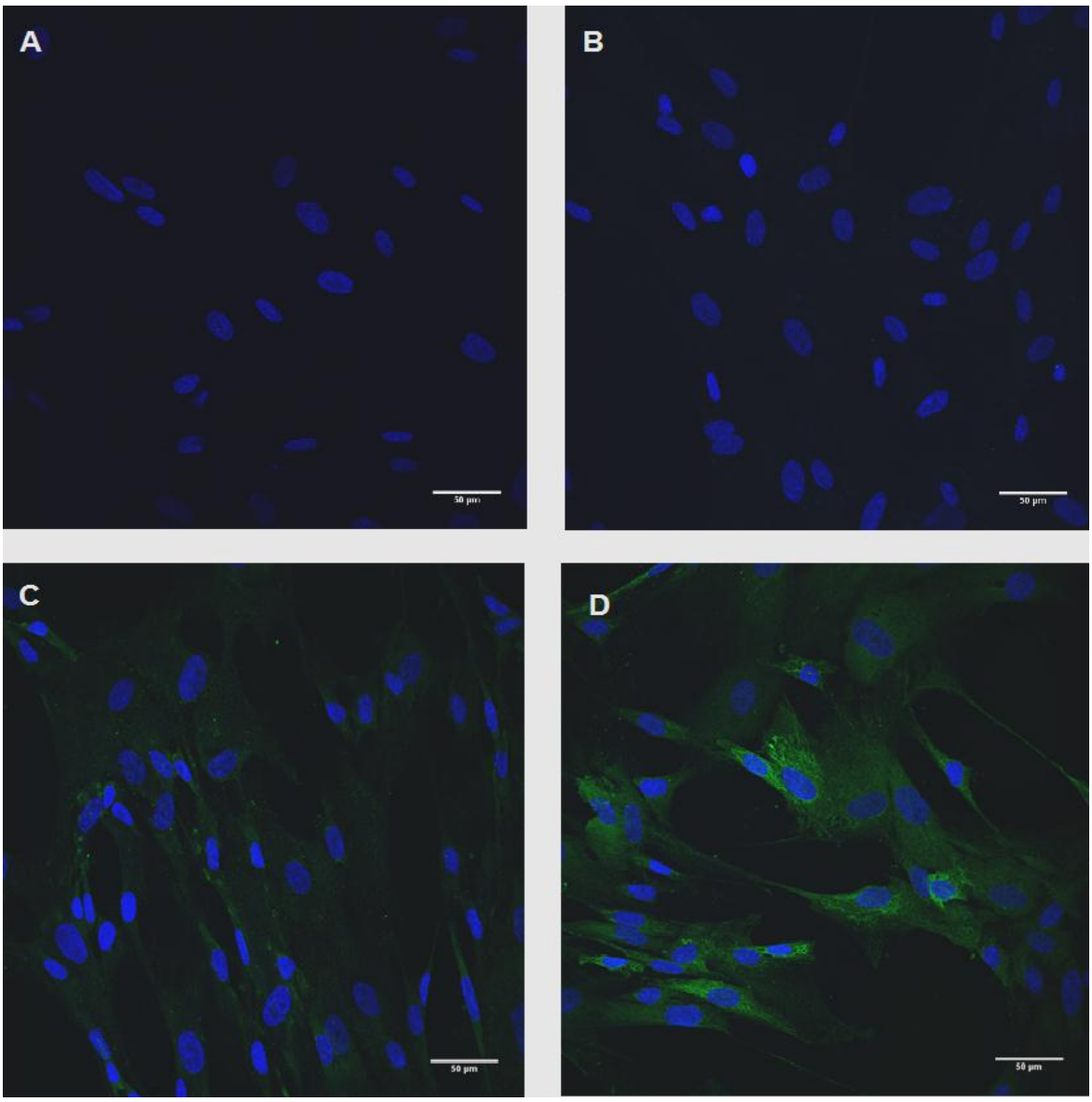

Figure 7. Immunostaining of CaSR in NHA subconfluent cultures in quiescent conditions. Images from a representative culture without (left) and with (right) permeabilization were taken by confocal microscopy. The nuclei are stained with DAPI (blue) and the CaSR protein is shown in green. The negative controls are shown in the upper panels (7A, B). The CaSR positive NHA subconfluent cultures are shown respectively in panels 7C and 7D. The images are taken with a 40x objective. Scale bar = 50 µm.

3.2. Morphological features of NHA subconfluent cultures upon incubation with Aβ42 or NPS-R-568

In order to evidence morphological alterations of the astrocyte cytoskeleton, NHA subcultures were incubated with 1, 10 or 20 μM Aβ42 for 6 (Fig. 8) or 12 hours (Fig. 9).

Resting cells incubated with vehicle (Fig. 8A, B, C) are heterogeneous in morphology as previously observed in resting conditions upon incubation with quiescent medium (Fig. 5). Most of the cells are polygonal in structure with less processes and a lower density (Fig. 8A, B). Besides, cells with long, fine processes and a lot of nuclei (Fig. 8C) were also observed under the same culture conditions. A few cell soma showed triangular morphology while others show irregular or rounded feature (Fig. 8B). In addition, astrocytes with elongated shape are also observed (Fig. 8C). The F-actin filaments within one cell looked parallel and oriented to one direction. There were no major differences seen between the subconfluent NHA cultures in resting conditions and the subcultures treated with vehicle.

Further, no differences were observed in the morphology of cultures in the presence of increasing concentrations of Aβ42 compared to control cultures. There was no typical reactive astrocyte morphology i.e. stellation and multiple process-bearing, seen in these cultures.

In the presence of 1 μM Aβ42, some cells showed long, thin processes and actin filaments were arranged longitudinally (Fig. 8D) while some other cells showed lower contrast and more nuclei without a visible cell body (Fig. 8D). Other cells looked very irregular and the F-actin filaments at the edges of the cells were slightly more intense than the ones in the middle of the cells (Fig. 8E), and sometimes the cells appear densely packed (Fig. 8F).

There was no major difference seen between cells treated with 1 μM and those treated with 10 μM Aβ42. Some cells showed a small cell body without processes (Fig. 8G, H) while other cells showed a triangular cell body and an extended process (Fig. 8I). Most of the F-actin filaments were pointing to one direction, however, some showed a criss-cross feature.

A decrease in cell density and a separation of the cells were observed in cells treated with 20 μM Aβ42 (Fig. 8J, K, L). These cells tend to move further from each other and form fine, elongated processes with shrunk cell bodies. The actin filaments were as well oriented parallel as in a crisscross manner.

Further, de visu difference between the treated and non-treated cells is hard to define. Besides, the cells did not show an equal intensity in staining. So there is no apparent difference between the vehicle and the treated cells at time 6 hours.The features of cell cultures visualized after 12 hours didn't differ a lot from those at 6 hours. There was no difference seen between the two time points at the fluorescence microscopy level.

Some cells looked stretched and carried sharp, reedy processes (Fig. 9A, B, C). As regards to structure these cells looked the same as cells treated with vehicle at 6 hours (Fig. 8A, B, C). As well in figure 8 as in figure 9 the majority of cells appeared flat and polygonal. No apparent difference in F-actin organization could be seen between time point 6 h and 12 h could be seen. Non-treated resting subconfluent NHA cultures at both time points showed the same kind of cells and cytoskeletal arrangement.

The 1 μM Aβ42 treated subcultures at 12 hour (Fig. 9D, E, F) did not differ from the subcultures at 6 hours (Fig. 8D, E, F). The majority of the cells looked extended and the actin filaments are organized longitudinally pointing to one direction.

A great number of the cells treated with 10 μM Aβ42 (9G, H, I) seemed to have long, fine processes and the actin filaments are rearranged in a crisscross manner. Some cells show a smaller cell body without any processes and others looked like spots. De visu there was no dissimilarity detected between the different time points of incubation with 10 μM Aβ42.

In contrast to the cells incubated with 20 μM Aβ42 at time point 6 hours (8J, K, L), the subcultures at 12 hours (9J, K, L) showed a higher cell density and the cell bodies did not look minimized. The cells showed narrow processes. However a clear de visu difference between the two time points is not clear. Besides, dissimilarity between treated and non-treated cells is hard to define.

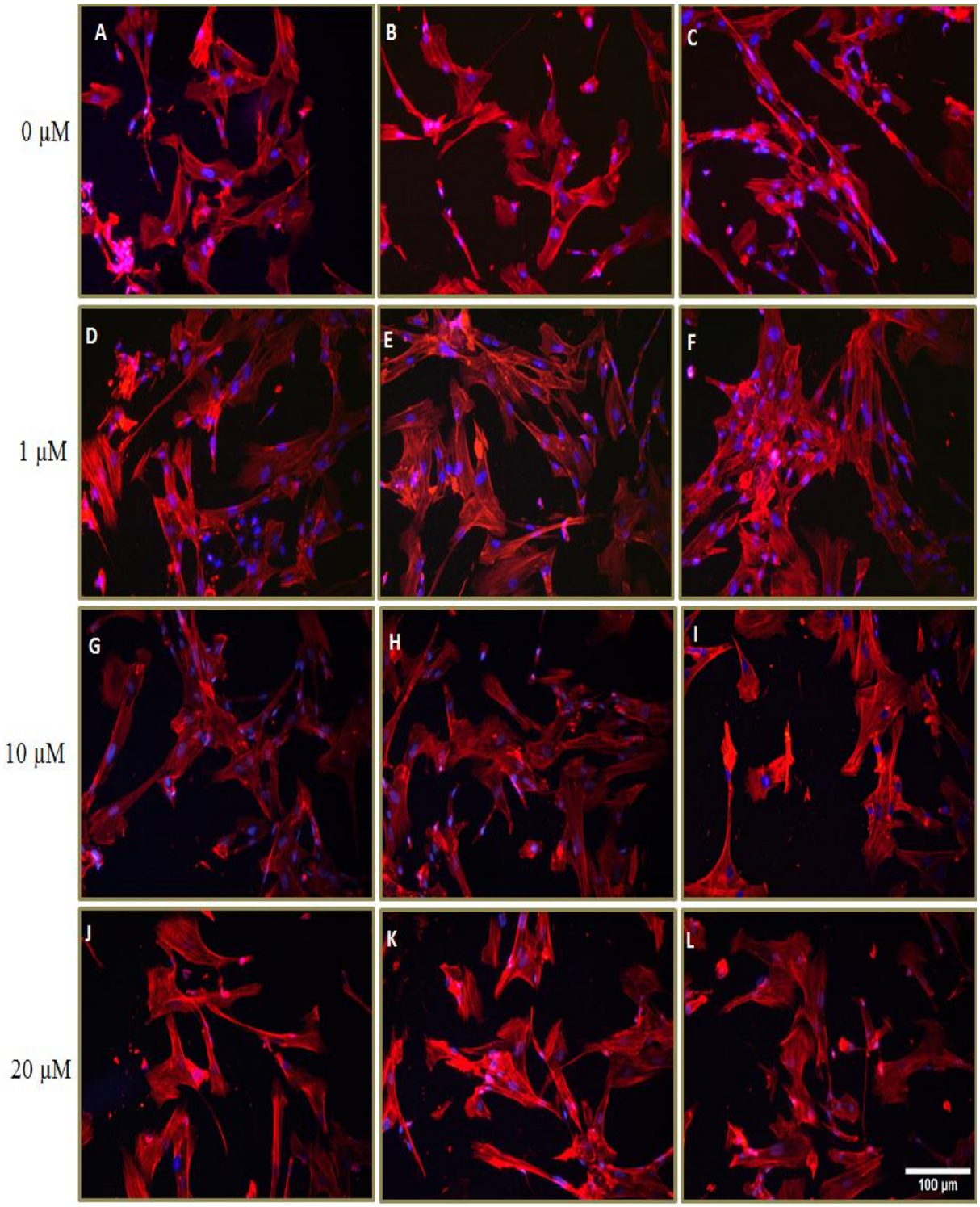

Figure 8. A representative view of resting NHA subcultures after 6 hours incubation in increasing concentrations of Aβ42. Three representative images per condition out of five different biological replicates are shown. The upper panels (A, B and C) show the non-treated subcultures (vehicle). The panels D, E and F characterise the cells treated with 1 µM Aβ42. The pictures G, H and I show the subcultures treated with 10 µM Aβ42 and the lower images (J, K and L) illustrate the cells treated with the highest concentration 20µM Aβ42. The nuclei are shown in blue (DAPI) and the F-actin cytoskeleton is stained red (TRITC-phalloidin). The images were taken with a 20x objective. Scale bar = 100 µm.

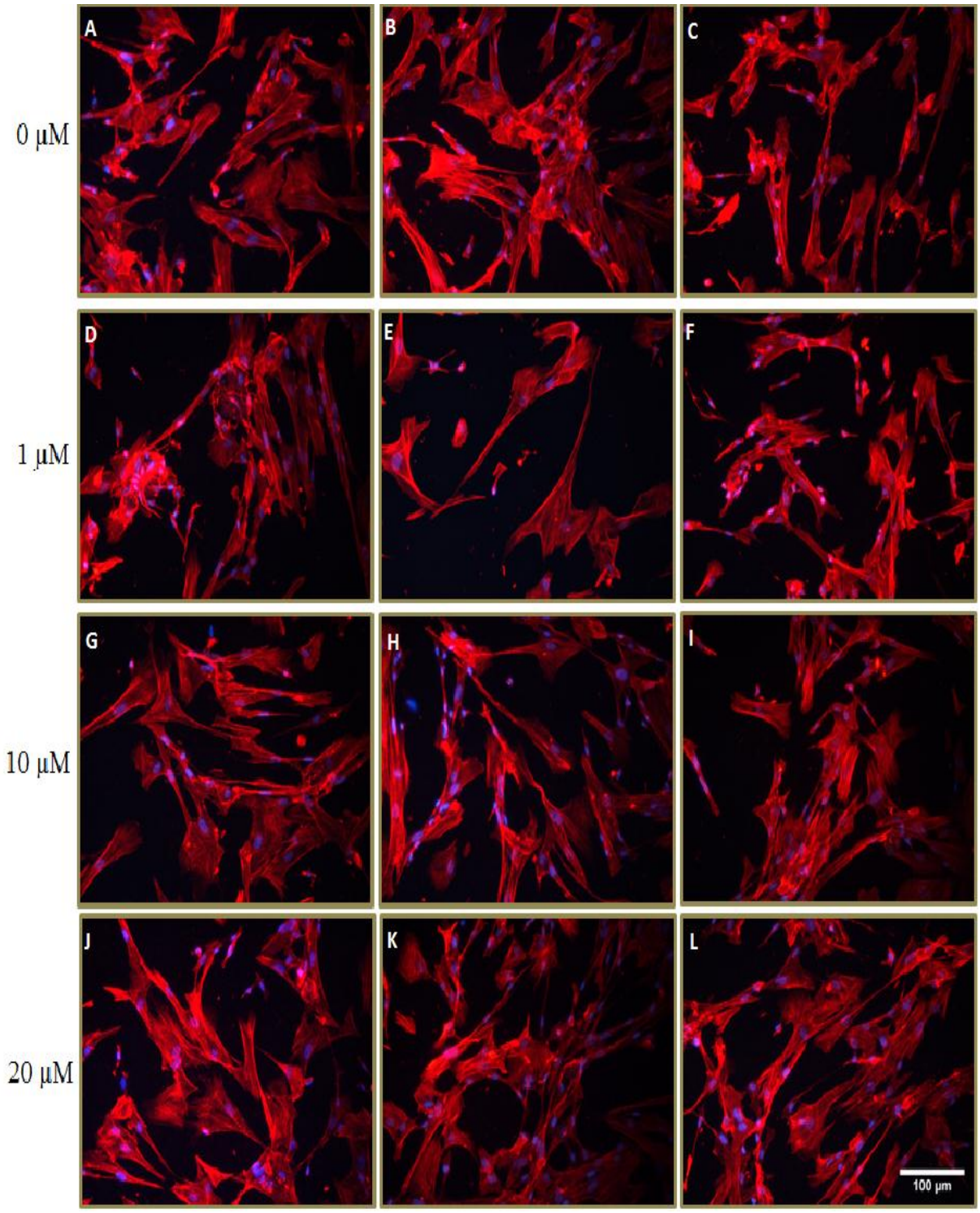

Figure 9. A representative view of resting NHA subcultures after 12 hours incubation in increasing concentrations of Aβ42. Three representative images per condition out of five different biological replicates are shown. The upper panels (A, B and C) show the non-treated subcultures (vehicle). Sections D, E and F illustrate the cells treated with 1 µM Aβ42 while G, H and I demonstrate the subcultures treated with 10 µM Aβ42. The lower images (J, K and L) represent the cells treated with the highest concentration of Aβ42 (20 µM). The nuclei are shown in blue (DAPI) and the actin cytoskeleton is coloured in red (TRITC-phalloidin). The images were taken with a 20x objective. Scale bar = 100 µm.

Further, no differences were observed in the morphology of cultures in the presence of increasing concentrations of NPS-R-568 compared to control cultures. The vehicle and NPS-R-568 treated cells after 6 hours and 12 hours respectively (Fig. 10, 11) were evaluated. The controls at both time points, 6 h (Fig. 10A, B, C) and12 h (Fig. 11A, B, C), looked slightly different from each other. In Fig. 10 the vehicle treated cultures showed elongated cells with long, narrow processes while in Fig. 11 the cells looked rather polygonal with shorter processes and some cells even did not show any processes.

The subcultures treated with 0.1 µM NPS-R-568 (Fig. 10D, E, F) displayed a decreased cell density. The cells seemed small, flat and shrunk. These cells showed rather a rounded appearance instead of polygonal while other cells at 12 h (Fig. 11D, E and F) showed high cell density and carried elongated processes.The NHA cells incubated for 6 hours with 1 µM NPS-R-568 (Fig. 10G, H, I) looked extended and carried long processes. However, at 12 h the cells showed less processes (Fig. 11G, H, I). With 10 µM of NPS-R-568 at 6 h, most of the cells (Fig. 10J, K and L) showed a flat, polygonal morphology with narrow processes, while at 12 h most of the cells displayed a triangular cell body with a thin process (Fig. 11J, K, L).

A general observation in subcultures treated with the agonist was a high presence of small, bright cytoplasmic vesicles with a high intensity also visible on the processes. On some confocal images (data not shown) these vesicles appeared individually while on others they were seen in clusters. These vesicles were also seen in vehicle and in Aβ42 treated subcultures but in a lower quantity. These vesicles could be the equivalent of the coated vesicles and caveolae observed by TEM.

Summarized, the NHA cells, treated with increased concentrations of Aβ42 or NPS-R-568 and evaluated at time points 6 hours and 12 hours, did not show any apparent difference in morphology. The treated cells also did not differ from non-treated or vehicle treated resting NHA cultures. Characteristic reactive cell morphology was not observed in these NHA subconfluent cultures. The treated subcultures did not show typical stellated, process-bearing feature. There was also no cytoplasmic retraction and rounding of the cell soma. In addition, the majority of the cells showed a parallel and well organized F-actin cytoskeleton, regardless differences in time point, concentration and the product used for treatment.

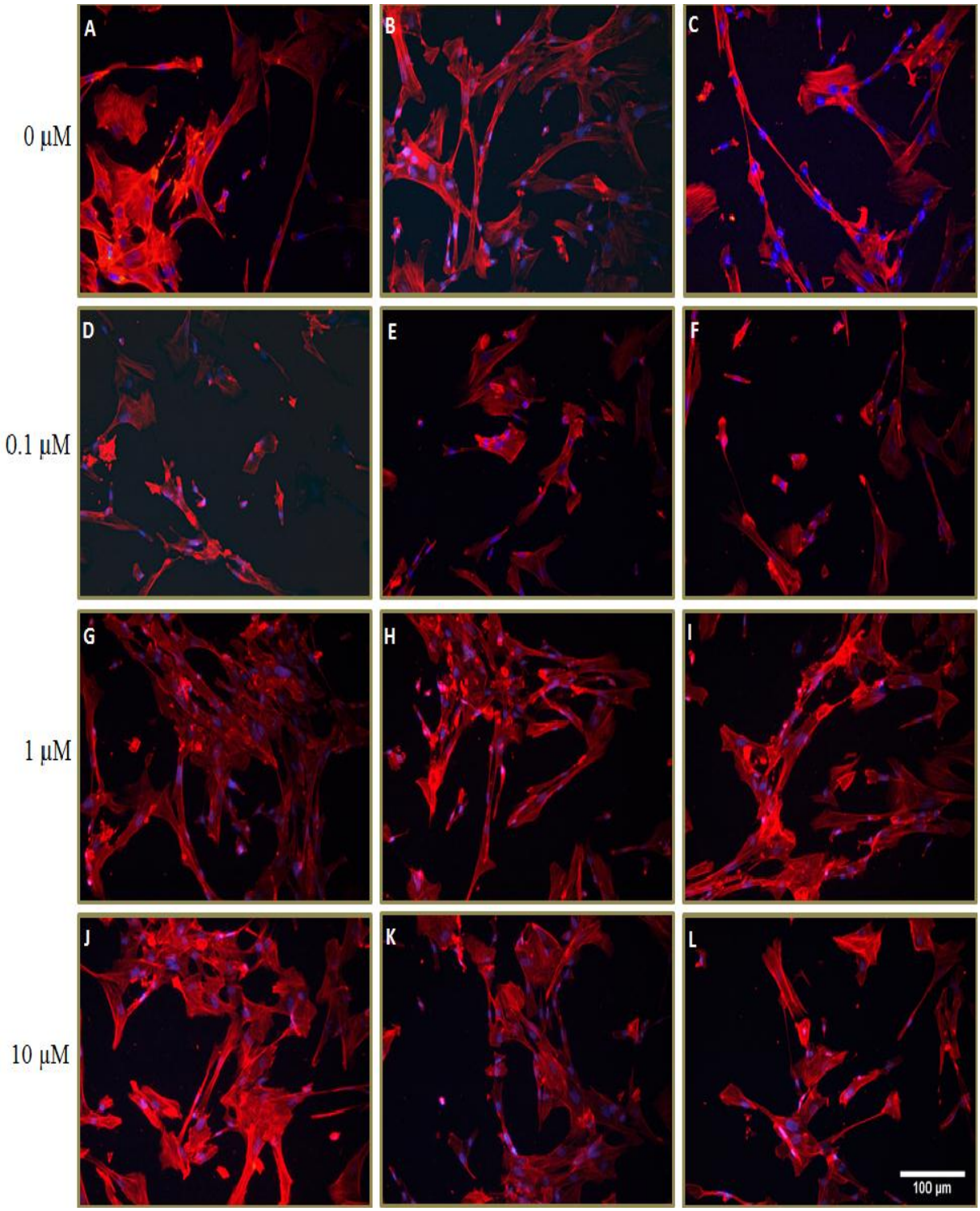

Figure 10. A representative view of resting NHA subcultures after 6 hours incubation in increasing concentrations of the agonist NPS-R-568. Three representative images per condition out of five different biological replicates are shown. The upper panels (A, B and C) show the non-treated subcultures (vehicle). The panels D, E and F represent the cells treated with 0.1 µM NPS-R-568 while G, H and I show the subcultures treated with 1 µM of NPS-R-568. The lower images (J, K and L) illustrate the cells treated with the highest concentration of agonist, 10 µM NPS-R-568. The nuclei are stained with DAPI (blue) and the actin cytoskeleton is stained with TRITC-phalloidin (red). The images were taken with a 20x objective. Scale bar = 100 µm.

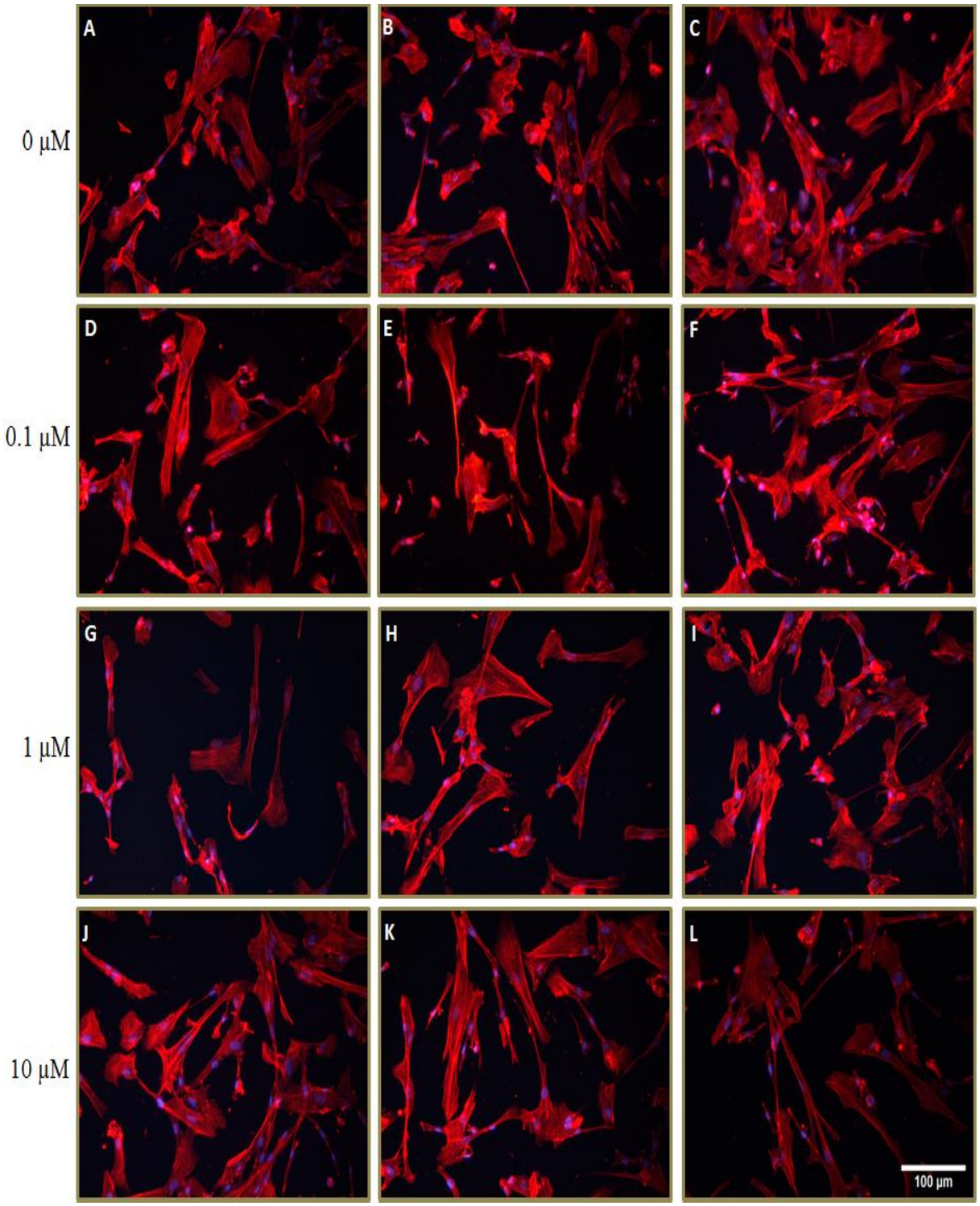

Figure 11. A representative view of resting NHA subcultures after 12 hours incubation in increasing concentrations of the agonist NPS-R-568. Three representative images per condition out of five different biological replicates are shown. The upper panels (A, B and C) show the non-treated subcultures (vehicle). The panels from D to F represent the cells treated with 0.1 µM NPS-R-568 while G, H and I show the subcultures treated with 1 µM of NPS-R-568. The lower images (J, K and L) are representing the cells treated with the highest concentration of agonist, 10 µM NPS-R-568. The nuclei are shown in blue (DAPI) and the actin cytoskeleton is stained with TRITC-phalloidin (red). The images were taken with a 20x objective. Scale bar = 100 µm.

3.3. IL-1β, TNF-α and iNOS mRNA levels in NHA subconfluent cultures upon addition of amyloid beta-42 or NPS-R-568

To determine the activation of NHA cells, we measured the mRNA levels of some pro-inflammatory mediators (IL-1β, TNF-α, iNOS) by qRT-PCR.

Two out of three experiments show a slight upregulation of IL-1β after 6 hours incubation with 1 µM Aβ42, with a high variation between the three experiments. When incubating with 10 µM and 20 µM Aβ42, no upregulation could be observed. In addition, no increase in IL-1β expression was seen for any culture 12 hours after incubation with different concentrations of Aβ42.

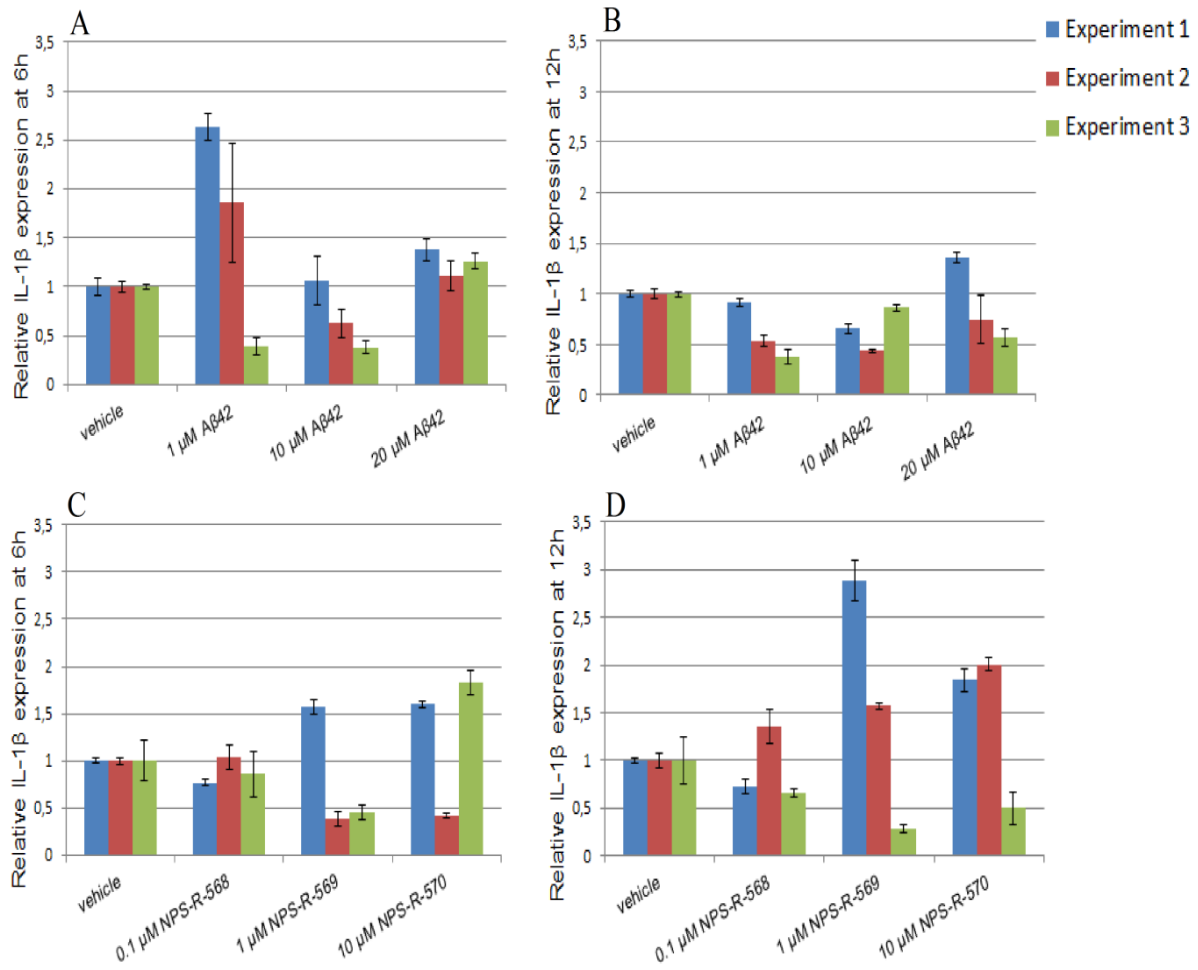

Figure 12. Effect of Aβ42- (A, B) and NPS-R-568- (C, D) induced IL-1β mRNA expression in NHA subconfluent cultures in quiescent conditions for 6 (A, C) and 12 hours (B, D) determined by qRT-PCR. Bars (blue = experiment 1, red = experiment 2 and green = experiment 3) represent the relative IL-1β mRNA levels of the mean ± standard deviation of three biological repeats in triplicate. The X-axis shows the different concentrations of either Aβ42 (A, B) or NPS-R-568 (C, D) while the Y-axis gives the relative IL-1β mRNA expression levels.

Among the three pro-inflammatory mediators (IL-1β, TNF-α and iNOS) which are produced by Aβ-evoked astroctyes, a constitutive expression could only be observed for IL-1β. However, no differences in IL-1β mRNA levels could be observed in any of the astrocyte subcultures incubated with the different concentrations of NPS-R-568 either for 6 or 12 hours (Fig.12C, D). In conclusion, NHA subcultures did not show any activation upon incubation with Aβ42 or NPS-R-568.

It has been previously reported that Aβ42 is able to activate mouse and human astrocytes *in vitro* [21,28]. Under the current experimental conditions, no activation of NHA cells, neither morphologically nor transcriptionally could be observed upon incubation in the presence of different concentrations of Aβ42.

3.4. Negative staining

In order to check whether the method that we followed to prepare the oligomeric form of Aβ42 was yielding the expected conformation, we performed a negative staining. An aliquot of the prepared Aβ42 solution was pipetted on a formvar coated grid. After staining the grids for 2 minutes, they were rinsed with milli-Q and air-dried. Transmission electron microscopy, as seen in figure 13, shows that we obtained spherical and protofibrillar oligomers, but not the fibrillar form according to the descriptions by Shin et al. [32].

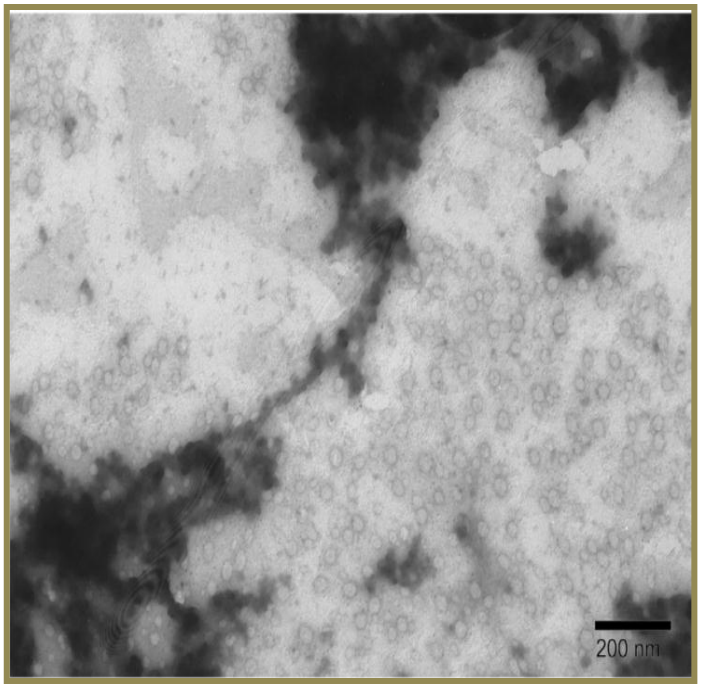

Figure 13. The oligomeric conformation of Aβ42 is shown with a negative staining. The spherical grey spots are the oligomers. The image is taken with a transmission electron microscope. Scale bar = 200 nm.

3.5. The results from GFAP staining

As the mature, responsive astrocytes are shown to be 70 to 90 percent positive for glial fibrillary acidic protein (GFAP), the NHA cells were tested for the expression of this protein. The subcultures in passage seven showed very low (5%) positivity for GFAP (data not shown).

4. Discussion

In these experiments we report the use of NHA subconfluent quiescent cultures to study the role of the CaSR in astrocyte activation induced by Aβ42. NHAs are astrocytes derived from the brain of a 22 weeks old human foetus.

To the best of our knowledge, expression of the CaSR in the cell line used for the current experiments has not been previously evaluated. Therefore, the presence of CaSR mRNA and protein was checked in NHA cultures. A moderate expression of the CaSR protein could be detected by immunofluorescence in the seventh subculture. This is in accordance with a previous report from Chattopadhyay et al. demonstrating the presence of CaSR protein in primary human astrocytes [21]. However, although the previous authors also found CaSR at transcriptional level, no detectable mRNA was found in different NHA subcultures (third to seventh passage) in our study. It is possible that CaSR mRNA levels were not detected in the current experiments due to the existence of a splice variant lacking the fourth exon, for which the primers/probe used in the current experiments were designed. The aforementioned report by Chattopadhyay et al. and another study by Brown et al. were able to detect mRNA of CaSR in human and mice astrocytes using primers designed in exon 7 and exon 5, respectively [21,33]. However, since a splice variant lacking exon 5 has been described [20] it is not recommended to use this region to evaluate total CaSR mRNA levels.

Typical astrocyte characteristics such as elongated mitochondria and extensions, high number of microvesicles and coated vesicles [34,35] were found in subconfluent quiescent cultures undergoing the seventh passage by transmission electron microscopy, demonstrating that the culture conditions and the subculture used for the experiments set up consisted mainly out of astrocytes.

In culture, proliferating astrocytes have a flat, polygonal shape [30,36]. When treated with an activating agent, astrocytes adopt a stellate, process-bearing morphology resembling their *in vivo* appearance. Stellation is accompanied by loss of actin stress fibers and focal adhesions [36]. In our study, the Aβ42 treated cells and their controls did not yield a de visu distinction between the vehicle control and the treated cells. No correlation is found between the cell morphology at one hand and the dose or time of incubation on the other hand. All subcultures contained a variety of cell configurations which were visible at each time point and each concentration of Aβ42. There was also no difference in morphology between the subcultures treated with the oligomeric Aβ42

and the subcultures treated with the agonist NPS-R-568. Although unlikely, we cannot exclude that a morphometric approach measuring cell area and stellation of cultured astrocytes after treatment with fibroblast growth factor (FGF-2) as described by Nagayasu et al. [37] would not have yielded significant differences.

Different research groups have previously demonstrated that cultured astrocytes can be activated by Aβ peptides in various species i.e. humans, mice and rats [21,28,30]. However, neither morphological nor transcriptional activation could be evidenced in the current experiments with NHAs subconfluent cultures. Only a slight increase in IL-1β could be observed for two out of three experiments 6 hours after incubation with 1 μM Aβ42 [Fig.12].

The poor activating response in the presence of Aβ42 *in vitro* compared to previously reported results could be in part due to interspecies variability, differences reported among Aβ batches, the form of Aβ and the maturation and plasticity status of astrocytes [38,39,40].

Indeed, human astrocytes have been previously shown to bind more avidly amyloid fibrils than their rat counterparts due to the differences in scavenger receptors on astrocytes which can adhere fibrillar and non-fibrillar Aβ peptides [39]. In addition, a difference in batch was also observed by Tapio Nuutinen et al. [41] comparing the effect of human fibrillar Aβ40 and Aβ42 to mouse fibrillar Aβ40 and Aβ42 peptides, upon cytoplasmic vacuole formation. The human Aβ42 fibrillized peptides induced clear cytoplasmic vacuole formation in cultured normal human astrocytes (NHA) and human CCFsttg1 astrocytoma cells while human fibrillar Aβ40 peptides as well as mouse Aβ42 peptides also induced a vacuolar response in human astrocytic cells but the extent was less than that seen with human fibrillized Aβ42 peptides.

Another explanation for the difference in responsiveness among astrocytes includes the maturation and plasticity status of astrocytes [40]. Astrocytes exhibit a high degree of plasticity in their phenotype by modifying their characteristics throughout life. For example, the morphology of astrocytes changes markedly during neuronal migration, maturation, and degeneration [40]. Evidence suggests that the expression of glial receptors may be developmentally regulated by both intrinsic and extrinsic signals. In addition, glial morphology can be reciprocally regulated by neurotransmitters such as norepinephrine and glutamate. This reciprocal regulation may be significant since both beta-adrenergic receptors and glutamate transporters are found predominantly in astrocytes in the brain [40].

Hu et al. [30] showed that the morphological changes, induced by Aβ42 in rat cultured astrocytes, were concentration-dependent. However, this treatment reached a maximal activation at a higher concentration of the oligomeric Aβ42 (20 μM) in humans, compared to mice and rat astrocytes that could be activated at 5-10 μM. Activation in rats and mice also occur faster with an evident activation by 3 to 6 h and reaching a peak at 12 h after addition of the Aβ42 peptide.

In current study constitutive expression of IL-1β was observed in the resting cultures. This has been previously observed in cultured astrocytes from mice and rats under serum-free conditions [28,30]. Although a slight upregulation of IL-1β mRNA was observed at 6 hour in the presence of 1 μM Aβ42, no differences were detected at any of the agonist NPS-R-568 concentrations at any time point.

It has been previously reported that incubation in the presence of CaSR agonists is able to mediate the release of pro-inflammatory mediators such as TNF-α and NO in kidney and Leydig cancer cells respectively [42,27]. Although, it would be possible that Aβ in the presence of CaSR agonist could have primed the expression of the pro-inflammatory mediators, this combination has not yet been tested. Additional experiments including combinations of Aβ and CaSR agonist or antagonist should be performed in order to further test the role of the CaSR in astrocyte activation induced by Aβ42.

Due to the lack of transcriptional and morphological response of NHA cells upon incubation with Aβ42 we initiated a quest for potential pitfalls. As the form of Aβ42 has been shown [30] to be important for proper activation of astrocytes, we checked the configuration of Aβ42 (see M&M) and tested whether the peptide was correctly aggregated. The negative staining of the Aβ42 confirmed that the preparation method yielded the required protofibrillar (non-fibrillar) or oligomeric form of Aβ42. Hu et al. [30] reported that oligomeric form of Aβ42 is more toxic and activates the cells higher than fibrillair or scrambled forms of Aβ42.

Since GFAP is an important marker for mature astrocytes, we first tested whether the cells are GFAP positive. GFAP is one of a family of intermediate filament proteins, including vimentin and nestin that serve largely cyto-architectural function. Intermediate filaments form networks that provide support and strength to cells. Although its function is not fully understood, GFAP is probably involved in controlling the shape, movement, and function of astroglial cells.

Different isoforms and splice variants of GFAP including GFAP a, b, c, d, and j have been described [13]. These may be expressed in a heterogeneous manner in both healthy CNS and in

pathological conditions but the differential distribution and roles of GFAP isoforms are only beginning to be studied. It is becoming evident that activation of glia cells can actually be accompanied by decreases in GFAP mRNA or protein. Hu et al. [30] showed that Aβ-treated astrocyte cultures exhibit a reorganized GFAP cytoskeleton, and condensed fluorescence intensity, which are typical for a reactive morphology. However, this treatment did not lead to an increase in GFAP levels [30]. Salinero et al. [29] reported that Aβ25-35 induced cytoskeletal reorganization and changes in GFAP immunoreactivity in cultured astrocytes but did not alter GFAP mRNA levels. These findings raise the question of whether induction of GFAP expression alone should be used as a suitable indicator for astrocyte activation.

Within the NHA subcultures used for the current study only 5% of the cells were positive for GFAP. This is very likely due to the fact that GFAP expression cannot be guaranteed above 10 cell doublings. In agreement with our results, it has been reported that due to stimulated cell division by passaging, astrocyte subcultures will mainly exhibit flat polygonal rather than process-bearing morphology [43]. In addition, it has been shown that cultured rat astrocytes are responsive to reactive agents when they are 70 to 80% GFAP positive [35]. It can be proposed that the decreased responsiveness of NHAs to Aβ is possibly related to the low GFAP expression in the subculture used.

5. Conclusion

In conclusion, Aβ42 and NPS-R-568 did neither affect the morphological features nor transcriptional expression of pro-inflammatory mediators of NHA quiescent subcultures. It is possible that GFAP negative astrocytes have a decreased responsiveness to certain activating compounds such as Aβ. Therefore, although the CaSR is expressed in NHAs, the role of CaSR in astrocyte activation induced by Aβ42 should be further studied in GFAP positive NHA cultures.

6. References

1. Blennow K, de Leon MJ, Zetterberg H (2006). Alzheimer's disease. Lancet 368:387-403.
2. Bekris LM, Yu CE, Bird TD, Tsuang DW (2011). Genetics of Alzheimer disease. Journal of geriatric psychiatry and neurology 23:213-227.
3. Perl DP (2000). Neuropathology of Alzheimer's disease and related disorders. Neurologic Clinics. 18:847-+.
4. Selkoe DJ. Alzheimer's Disease (2011). Cold Spring Harbor Perspectives in Biology 3(7)
5. Goedert M, Spillantini MG (2006). A century of Alzheimer's disease. Science 314: 777-781.
6. Serrano-Pozo A, Frosch MP, Masliah E, Hyman BT (2011). Neuropathological Alterations in Alzheimer Disease. Cold spring Harbor Perspectives in Biology 3(12)
7. Maltsev AV, Bystryak S, Galzitskaya OV (2011). The role of beta-amyloid peptide in neurodegenerative diseases. Ageing Research Reviews 10:440-452.
8. Hicks DA, Nalivaeva NN, Turner AJ (2012). Lipid rafts and Alzheimer's disease: protein-lipid interactions and perturbation of signaling. Frontiers in physiology 3:189.
9. Schaeffer EL, Figueiro M, Gattaz WF (2011). Insights into Alzheimer disease pathogenesis from studies in transgenic animal models. Clinics 66:45-54.
10. Gotz J, Streffer JR, David D (2004). Transgenic animal models of Alzheimer's disease and related disorders: histopathology, behavior and therapy. Molecular Psychiatry 9:664-683
11. Janus C, Westaway D (2001). Transgenic mouse models of Alzheimer's disease. Physiology and Behaviour 73:873-886.
12. Matyash V, Kettenmann H (2010). Heterogeneity in astrocyte morphology and physiology. Brain research reviews 63:2-10.
13. Sofroniew MV, Vinters HV (2010). Astrocytes: biology and pathology. Acta Neuropathologica 119:7-35.
14. Li CY, Zhao R, Gao K (2011). Astrocytes: Implications for Neuroinflammatory Pathogenesis of Alzheimer's Disease. Current Alzheimer Research 8:67-80.
15. Blasko I, Veerhuis R, Stampfer-Kountchev M, Saurwein-Teissl M, Eikelenboom P, Grubeck-Loebenstein B (2000). Costimulatory effects of interferon-gamma and interleukin-1beta or tumor necrosis factor alpha on the synthesis of Abeta1-40 and Abeta1-42 by human astrocytes. Neurobiology of disease 7:682-689.
16. Rubio-Perez JM, Morillas-Ruiz JM (2012). A review: inflammatory process in Alzheimer's disease, role of cytokines. TheScientificWorld Journal 2012:1-15.

17. Yano S, Brown EM, Chattopadhyay N (2004). Calcium-sensing receptor in the brain. Cell calcium 35:257-264.

18. Conley YP, Mukherjee A, Kammerer C (2009). Evidence supporting a role for the calcium-sensing receptor in Alzheimer disease. American journal of medical genetics. Part B, Neuropsychiatric genetics 150B:703-709.

19. Diez-Fraile A, Mussche S, Vanden Berghe T, Espeel M, Vandenabeele P, D'Herde KG (2010). Expression of calcium-sensing receptor in quail granulosa explants: a key to survival during folliculogenesis. Anatomical record 293:890-899.

20. Brown EM, MacLeod RJ (2001). Extracellular calcium sensing and extracellular calcium signaling. Physiological reviews 81:239-297.

21. Chattopadhyay N, Evliyaoglu C, Heese O (2000). Regulation of secretion of PTHrP by Ca(2+)-sensing receptor in human astrocytes, astrocytomas, and meningiomas. American Journal of Physiology. Cell physiology 279:C691-699.

22. Hu J, Reyes-Cruz G, Goldsmith PK, Gantt NM, Miller JL, Spiegel AM (2007). Functional effects of monoclonal antibodies to the purified amino-terminal extracellular domain of the human Ca(2+) receptor. Journal of bone and mineral research 22:601-608.

23. Jensen AA, Brauner-Osborne H (2007). Allosteric modulation of the calcium-sensing receptor. Current neuropharmacology 5:180-186.

24. Magno AL, Ward BK, Ratajczak T (2011). The calcium-sensing receptor: a molecular perspective. Endocrine reviews 32:3-30.

25. Ye C, Ho-Pao CL, Kanazirska M (1997). Amyloid-beta proteins activate Ca(2+)-permeable channels through calcium-sensing receptors. Journal of neuroscience research 47:547-554.

26. Dal Pra I, Chiarini A, Nemeth EF, Armato U, Whitfield JF (2005). Roles of Ca^{2+} and the Ca^{2+}-sensing receptor (CASR) in the expression of inducible NOS (nitric oxide synthase)-2 and its BH4 (tetrahydrobiopterin)-dependent activation in cytokine-stimulated adult human astrocytes. Journal of cellular biochemistry 96:428-438.

27. Tfelt-Hansen J, Ferreira A, Yano S (2005). Calcium-sensing receptor activation induces nitric oxide production in H-500 Leydig cancer cells. American journal of physiology. Endocrinology and metabolism 288:E1206-1213.

28. Zhao J, O'Connor T, Vassar R (2011). The contribution of activated astrocytes to Aβ production: implications for Alzheimer's disease pathogenesis. Journal of neuroinflammation 8:150-167.

29. Salinero O, Moreno-Flores MT, Ceballos ML, Wandosell F (1997). beta-Amyloid peptide induced cytoskeletal reorganization in cultured astrocytes. Journal of neuroscience research 47:216-223.

30. Hu J, Akama KT, Krafft GA, Chromy BA, Van Eldik LJ (1998). Amyloid-beta peptide activates cultured astrocytes: morphological alterations, cytokine induction and nitric oxide release. Brain research 785:195-206.

31. Dell'Aquila ME, De Santis T, Cho YS (2006). Localization and quantitative expression of the calcium-sensing receptor protein in human oocytes. Fertility and sterility 1:1240-1247.

32. Shin TM, Isas JM, Hsieh CL (2008). Formation of soluble amyloid oligomers and amyloid fibrils by the multifunctional protein vitronectin. Molecular neurodegeneration 3:16.

33. Chattopadhyay N, Espinosa-Jeffrey A, Tfelt-Hansen J (2008). Calcium receptor expression and function in oligodendrocyte commitment and lineage progression: potential impact on reduced myelin basic protein in CaR-null mice. Journal of neuroscience research 86:2159-2167.

34. Rohl C, Lucius R, Sievers J (2007). The effect of activated microglia on astrogliosis parameters in astrocyte cultures. Brain research 1129:43-52.

35. Qin AP, Liu CF, Qin YY (2010). Autophagy was activated in injured astrocytes and mildly decreased cell survival following glucose and oxygen deprivation and focal cerebral ischemia. Autophagy 6:738-753.

36. Ramakers GJA, Moolenaar WH (1998). Regulation of astrocyte morphology by RhoA and lysophosphatidic acid. Experimantal Cell Research 245:252-262.

37. Nagayasu T, Miyata S, Hayashi N, Takano R, Kariya Y, Kamei K (2005). Heparin structures in FGF-2-dependent morphological transformation of astrocytes. Journal of Biomedical Materials Research 74A:374-380.

38. Barnea A, Roberts J, Keller P, Word RA (2001). Interleukin-1 beta induces expression of neuropeptide Y in primary astrocyte cultures in a cytokine-specific manner: induction in human but not rat astrocytes. Brain research 896:137-145.

39. Alarcon R, Fuenzalida C, Santibanez M, von Bernhardi R (2005). Expression of scavenger receptors in glial cells. Comparing the adhesion of astrocytes and microglia from neonatal rats to surface-bound beta-amyloid. The Journal of biological chemistry 280:30406-30415.

40. Shao Y, McCarthy KD (1994). Plasticity of astrocytes. Glia 11:147-155.

41. Nuutinen T, Huuskonen J, Suuronen T, Ojala J, Miettinen R, Salminen A (2007). Amyloid-beta 1-42 induced endocytosis and clusterin/apoJ protein accumulation in cultured human astrocytes. Neurochemistry international 50:540-547.

42. Wang D, Pedraza PL, Abdullah HI, McGiff JC, Ferreri NR (2002). Calcium-sensing receptor-mediated TNF production in medullary thick ascending limb cells. American Journal of Physiology. Renal physiology 283:F963-970.

43. Vanzani MC, Iacono RF, Alonso A, Berria MI (2003). Immunochemical expression of proliferative cell nuclear antigen in aging cultured astrocytes. Medicina 63:303-306.

APPENDIX

Abbreviation list

AD	Alzheimer’s disease
AGM	Astrocyte Growth Medium
APP	Amyloid Precursor Protein
Aβ	Amyloid-beta
AICD	APP Intracellular Domain
APOE	Apolipoprotein E
BACE	Beta-site APP Cleaving Enzyme
Ca^{2+}_{i}	intracellular calcium
CaSR	Calcium-Sensing Receptor
CNS	Central Nervous System
CTF38	C-terminal Fragment 38
CTF99	C-terminal Fragment 99
DABCO	1,4-diaza-bicyclo(2.2.2)octane
DAPI	4',6-diamidino-2-phenylindole
DMSO	Dimethyl sulfoxide
D-PBS	Dulbecco Phosphate -Buffered Saline
EOAD	Early Onset Alzheimer’s disease
ER	endoplasmatic reticulum
ECD	Extracellular Domain
FBS	Fetal bovine serum
FGF-2	Fibroblast growth factor-2
GA	gentamicin
GFAP	Glial Fibrillary Acidic Protein
GPCR	G-protein coupled receptor

HFIP	1,1,1,3,3,3-hexafluoro-2-propanol
IL-1β	Interleukin-1-beta
iNOS	induced Nitric Oxid Synthase
IP	Inositol Phosphate
IP3	Inositol triphosphate
LOAD	Late Onset Alzheimer's disease
NHA	Normal Human Astrocyte
NFTs	Neurofibrillary Tangles
NPS-R-568	N-(3-[2-chlorophenyl]propyl)-(R)-a-methyl-3-methoxybenzylamine
PFA	Paraformaldehyde
PLC	Phospholipase C
PSEN1	Presinilin-1
PSEN2	Presinilin-2
PTH	Parathyroid Hormone
qRT-PCR	quantitative Reverse Transcription Polymerase Chain Reaction
rhEGF	recombinant human epidermal growth factor
sAPP-α	soluble Amyloid Precursor Protein-alfa
sAPP-β	soluble Amyloid precursor Protein-beta
TEM	Transmission Electron Microscopy
TNF-α	Tumor Necrosis Factor-alfa
TRITC	Tetramethylrhodamine
UTR	Untranslated region
VFT	Venus Fly Trap

Samenvatting

De ziekte van Alzheimer (AD) is de meest voorkomende irreversibele, progressieve vorm van dementie. Het wordt gekenmerkt door een geleidelijk verlies van geheugen en cognitieve vaardigheden. AD is goed voor meer dan 50% van alle gevallen van dementie, en vandaag zijn meer dan 35,6 miljoen mensen wereldwijd getroffen. Pathologische criteria, voor de diagnose van AD bij autopsie, zijn de aanwezigheid van neurofibrillaire tangles in de neuronen en seniele plaques tussen de neuronen. Seniele plaques zijn hoofdzakelijk samengesteld uit aggregaten van amyloïd-beta (Aβ) peptiden.

Verschillende onderzoeken hebben aangetoond dat de accumulatie van Aβ peptiden rondom de neuronen verantwoordelijk is voor AD. Het Aβ stimuleert de astrocyten waardoor, naast astrocytaire Aβ ook pro-inflammatoire mediatoren zoals interleukin (IL)-1β, tumor necrosis factor (TNF-α) en induced nitric oxid synthase (iNOS) vrijkomen.

Bovendien verschillende studies suggereren dat Aβ is betrokken bij de verstoring van cytosolische calcium homeostase. Dus mechanismen die verantwoordelijk zijn voor het handhaven van intracellulair calcium niveaus, waaronder de calcium-sensing receptor (CaSR), kunnen bijdragen tot de pathogenese van AD. Daarnaast is het reeds aangetoond dat Aβ de astrocyten kan activeren en functioneert als een CaSR agonist. Het belangrijkste doel van dit werk was om de rol van CaSR in astrocyten activatie te achterhalen.

Het is reeds gerapporteerd dat Aβ een sterk reactief fenotype in astrocyten induceert waarbij de vlakke polygonale vorm van astrocyten verandert in stervormig, proces-dragende morfologie en een cytoskeletale reorganisatie optreedt.

In dit onderzoek evalueerden we eerst de expressie van CaSR in normale menselijke astrocyten (NHAs). Nadien zijn we op zoek gegaan naar de morfologische verandering van NHAs bij incubatie met Aβ42 of CASR agonist-NPS R-568. Als laatste, onderzochten we de secretie van belangrijke pro-inflammatoire mediatoren (IL-1β, iNOS, TNF-α) die worden vrijgesteld door astrocyten na activering met Aβ.

Op basis van deze experimenten hebben we geconcludeerd dat Aβ42 en NPS-R-568 geen invloed uitoefenen noch op de morfologische kenmerken noch op transcriptionele expressie van pro-inflammatoire mediatoren van NHA subculturen.